J. Fluid Mech. (2017), *vol.* 828, *pp.* 318–352.
doi:10.1017/jfm.2017.502

Multiple phoretic mechanisms in the self-propulsion of a Pt-insulator Janus swimmer

Yahaya Ibrahim[1], Ramin Golestanian[2] and Tanniemola B. Liverpool[1,3,†]

[1]School of Mathematics, University of Bristol, University Walk, Bristol BS8 1TW, UK

[2]Rudolf Peierls Centre for Theoretical Physics, 1 Keble Road, Oxford OX1 3NP, UK

[3]BrisSynBio, Tyndall Avenue, Bristol BS8 1TQ, UK

(Received 31 March 2016; revised 6 July 2017; accepted 17 July 2017;
first published online 4 September 2017)

We present a detailed theoretical study which demonstrates that electrokinetic effects can also play a role in the motion of metallic-insulator spherical Janus particles. Essential to our analysis is the identification of the fact that the reaction rates depend on Pt-coating thickness and that the thickness of coating varies from pole to equator of the coated hemisphere. We find that their motion is due to a combination of neutral and ionic-diffusiophoretic as well as electrophoretic effects whose interplay can be changed by varying the ionic properties of the fluid. This has great potential significance for optimizing performance of designed synthetic swimmers.

Key words: biological fluid dynamics, micro-/nano-fluid dynamics, propulsion

1. Introduction

In recent years there has been a flurry of activity in developing micro- and nanoscale self-propelling devices that are engineered to produce enhanced motion within a fluid environment (Kapral 2013). They are of interest for a number of reasons, including the potential to perform transport tasks (Patra *et al.* 2013) and exhibit new emergent phenomena (Volpe *et al.* 2011; Theurkauff *et al.* 2012; Bricard *et al.* 2013; Kümmel *et al.* 2013; Marchetti *et al.* 2013; Palacci *et al.* 2013). A variety of subtly different methods, all based on the catalytic decomposition of dissolved fuel molecules, have been shown to produce autonomous motion or swimming. Commonly studied systems are catalytic bimetallic rod-shaped devices (Kline *et al.* 2005*b*) and metallic-insulator spherical Janus particles that are half-coated with catalyst (e.g. platinum) for a non-equilibrium reaction (e.g. the decomposition of hydrogen peroxide) (Howse *et al.* 2007) (see figure 1*a*). The propulsion mechanism is thought to be phoretic in nature (Anderson 1989; Golestanian, Liverpool & Ajdari 2007), but many specific details, such as which type of phoretic mechanism drive propulsion, remain the subject of debate (Golestanian *et al.* 2007; Gibbs & Zhao 2009; Brady 2011; Moran & Posner 2011). A fundamental understanding of the mechanisms is key for developing the knowledge of how to use and control them

† Email address for correspondence: t.liverpool@bristol.ac.uk

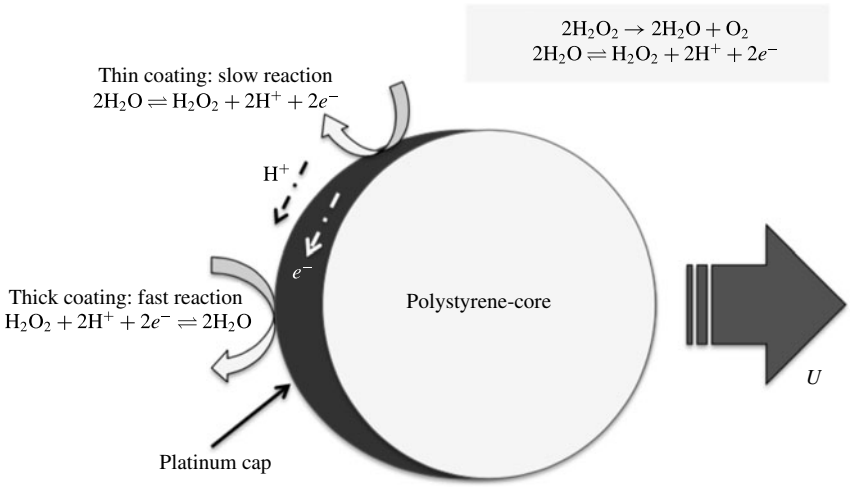

FIGURE 1. Cross-section of a schematic swimmer showing the variation of the thickness of the Pt-coating, the directions of the currents and swimming direction.

in applications and how to build up a picture of the collective behaviour through implementation of realistic interactions between catalytic colloids.

For bimetallic swimmers, a plausible proposal is that the two metallic segments, usually platinum and gold, electrochemically reduce the dissolved fuel in a process that results in electron transfer across the rod (Paxton, Sen & Mallouk 2005; Kagan *et al.* 2009). This, together with proton movement in the solution (Farniya *et al.* 2013) and the interaction between the resulting self-generated electric field and the charge density on the rod, produces (self-electrophoretic) motion (Moran & Posner 2011). The direction of travel and swimming speed for arbitrary pairs of metals are well understood in the context of this mechanism (Wang *et al.* 2006), as well as the link between fuel concentration and velocity (Sabass & Seifert 2012). For Pt-insulator Janus particles, the absence of conduction between the two hemispheres suggests a mechanism independent of electrokinetics. Hence, a natural first proposal is that a self-generated gradient of product and reactants can lead to motion via self-diffusiophoresis (Golestanian, Liverpool & Ajdari 2005), provided the colloid is sufficiently small (Gibbs & Zhao 2009). A number of predictions have been made based on this mechanism (Golestanian *et al.* 2005; Rückner & Kapral 2007; Popescu, Dietrich & Oshanin 2009; Sabass & Seifert 2010; Valadares *et al.* 2010; Brady 2011; Sharifi-Mood, Koplik & Maldarelli 2013) which have to date shown good agreement with the experimental dependency of swimming velocity on the size of the colloid (Ebbens *et al.* 2012) and fuel concentration (Howse *et al.* 2007). It would thus appear that a key difference between the bimetallic and metallic-insulator Janus particles is that the motility in the latter system does not require conduction or electrostatic effects. However recent experiments have raised the possibility that this assumption might not be completely correct (Brown & Poon 2014; Ebbens *et al.* 2014; Das *et al.* 2015).

Here we present a detailed theoretical study which demonstrates however that electrokinetic effects (Pagonabarraga, Rotenberg & Frenkel 2010) can also play a role in the motion of metallic-insulator spherical Janus particles expanding on our previous analyses briefly presented in Ebbens *et al.* (2014). We find that their motion

is due to a combination of neutral and ionic-diffusiophoretic as well as electrophoretic effects whose interplay can be changed by varying the ionic properties of the fluid (see figure 8). This has great potential significance as the effect on the swimming behaviour, of solution properties such as temperature (Balasubramanian *et al.* 2009), contaminants (Zhao *et al.* 2013), pH and salt concentration are of critical importance to potential applications (Patra *et al.* 2013).

We consider a Janus polystyrene (insulating) spherical colloid of radius a, half-coated by a platinum (conducting) shell. It is known that such colloids are active i.e. self-propel in hydrogen peroxide solution. This is due to gradients generated by the asymmetric decomposition of H_2O_2 on the Pt-coating and the interaction of the reactants and products with the sphere surface. In the rest of the paper we will call this process self-phoresis.

Generically, the catalytic decomposition of the hydrogen peroxide by the platinum catalyst is given by

$$\mathrm{Pt} + 2\mathrm{H_2O_2} \rightarrow \boxed{\texttt{Intermediate-complexes}} \rightarrow \mathrm{Pt} + 2\mathrm{H_2O} + \mathrm{O_2}, \tag{1.1}$$

however there is still some debate about the nature of the intermediate complexes Hall, Khudaish & Hart (1998, 1999*a*,*b*), Katsounaros *et al.* (2012).

In this article, we outline a detailed calculation of the self-phoresis problem. Our approach is guided by the well-studied problem of a phoretic motion of a colloid in an externally applied concentration gradient or electric field. To model the effect of the non-equilibrium chemical reaction sketched above on the motion of the Janus particle, we study the concentration fields of all the species involved in the reaction. The half-coating of the colloid by catalyst is reflected by inhomogeneous reactive boundary conditions on its surface. The reaction involves the production of charged intermediates which can also lead to changes in the electric potential on the swimmer surface and hence the possibility of local electric fields. Our flexible calculation framework allows us to study a variety of different schemes for the reaction kinetics of the intermediate complexes. Using this we analyse in detail a scheme with both charged and uncharged pathways (see appendix A) whose results are consistent with all the behaviour observed in the recent experiments.

2. The model

A Janus sphere of radius a has the catalytic reaction of hydrogen peroxide decomposition occurring on its Pt coated half. We choose, without loss of generality, that the normal to the plane splitting the hemispheres is aligned with the z-axis (see figure 2). We propose a theoretical framework based on generally accepted properties of the reaction scheme for Pt catalysis of H_2O_2 degradation to water and O_2 (Hall *et al.* 1998, 1999*a*,*b*). A key feature of our analysis of self-propulsion is that it takes account of the existence of charged intermediates within the catalytic reaction scheme, namely protons and that the reaction rates varies with the Pt coating thickness (see figure 1).

The state of the system is therefore described by the local state of the Pt on the coated hemisphere, the electric potential, $\bar{\Phi}(\bar{\boldsymbol{r}})$, the fluid velocity, $\bar{\boldsymbol{v}}(\bar{\boldsymbol{r}})$, the local concentrations, $\bar{c}_{hp}(\bar{\boldsymbol{r}})$, $\bar{c}_o(\bar{\boldsymbol{r}})$, $\bar{c}_h(\bar{\boldsymbol{r}})$ of H_2O_2, O_2 and H^+ respectively, i.e. the various reactive species, and the local concentrations, $\bar{c}_{oh}(\bar{\boldsymbol{r}})$, $\bar{c}_s(\bar{\boldsymbol{r}})$ of hydroxide and salt ions, respectively. The background concentrations (far from the Janus sphere) of the salt, H_2O_2, H^+ and OH^- are c_s^∞, c_{hp}^∞, c_h^∞, c_{oh}^∞ respectively. Positions outside the

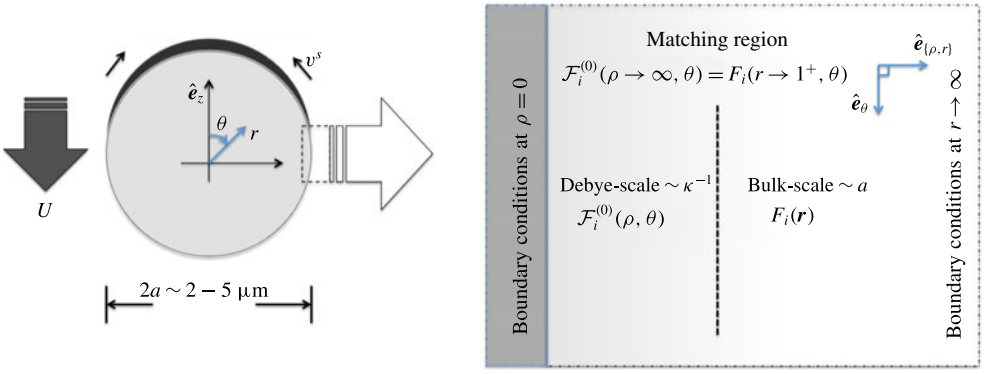

FIGURE 2. (Colour online) Schematic platinum–polystyrene swimmer and the domain decomposition of the phoretic problem.

Janus sphere (in the bulk) are represented by the vectors $\bar{\boldsymbol{r}} = (\bar{x}, \bar{y}, \bar{z})$ (in Cartesian coordinates) while positions on the surface are parametrized by the unit vectors $\hat{\boldsymbol{n}} = (\sin\theta\cos\phi, \sin\theta\sin\phi, \cos\theta)$. We note that the vector $\bar{\boldsymbol{r}} = (\bar{r}, \theta, \phi)$ and $\hat{\boldsymbol{n}} = \hat{\boldsymbol{e}}_{\bar{r}}$ in spherical polar coordinates. Each of the neutral species interacts non-electrostatically with the surface of the swimmer via a fixed short-ranged potential energy $\bar{\Psi}_n(\bar{\boldsymbol{r}})$, that depends on the distance from the Janus sphere surface. The interaction range, L_{eff} is taken to be the same for all neutral species.

2.1. *Equations of motion*

The relevant equations are Nernst–Planck equations (Probstein 2003) for the concentration of charged species, $\bar{c}_q$,

$$\partial_{\bar{t}}\bar{c}_q = -\bar{\boldsymbol{\nabla}}\cdot\bar{\boldsymbol{J}}_q; \quad \bar{\boldsymbol{J}}_q = -D_q\bar{\boldsymbol{\nabla}}\bar{c}_q + \bar{\boldsymbol{u}}_q\bar{c}_q; \quad \bar{\boldsymbol{u}}_q = \bar{\boldsymbol{v}} - \frac{D_q z_q e}{k_B T}\bar{\boldsymbol{\nabla}}\bar{\Phi}, \tag{2.1a–c}$$

drift-diffusion equations (Chandrasekhar 1943) for the neutral species, $\bar{c}_n$,

$$\partial_{\bar{t}}\bar{c}_n = -\bar{\boldsymbol{\nabla}}\cdot\bar{\boldsymbol{J}}_n; \quad \bar{\boldsymbol{J}}_n = -D_n\bar{\boldsymbol{\nabla}}\bar{c}_n + \bar{\boldsymbol{u}}_n\bar{c}_n; \quad \bar{\boldsymbol{u}}_n = \bar{\boldsymbol{v}} - \frac{D_n}{k_B T}\bar{\boldsymbol{\nabla}}\bar{\Psi}_n, \tag{2.2a–c}$$

Poisson's equation (Jackson 1975) for the electric potential

$$\bar{\nabla}^2\bar{\Phi} = -\sum_q \frac{z_q e\bar{c}_q}{\epsilon} \tag{2.3}$$

and the incompressible Navier–Stokes equations (Lamb 1932) for the fluid velocity

$$\left.\begin{aligned} \rho(\partial_{\bar{t}}\bar{\boldsymbol{v}} + \bar{\boldsymbol{v}}\cdot\bar{\boldsymbol{\nabla}}\bar{\boldsymbol{v}}) = \eta\bar{\nabla}^2\bar{\boldsymbol{v}} - \bar{\boldsymbol{\nabla}}\bar{p} + \bar{\boldsymbol{f}}(\bar{\boldsymbol{r}}); \quad \bar{\boldsymbol{\nabla}}\cdot\bar{\boldsymbol{v}} = 0, \\ \bar{\boldsymbol{f}}(\bar{\boldsymbol{r}}) = \sum_q \Gamma_q\bar{c}_q(\bar{\boldsymbol{u}}_q - \bar{\boldsymbol{v}}) + \sum_n \Gamma_n\bar{c}_n\,(\bar{\boldsymbol{u}}_n - \bar{\boldsymbol{v}})\,; \quad \Gamma_q = \frac{k_B T}{D_q}, \quad \Gamma_n = \frac{k_B T}{D_n}, \end{aligned}\right\} \tag{2.4}$$

where $\bar{p}(\bar{\boldsymbol{r}})$ is the hydrostatic pressure at $\bar{\boldsymbol{r}}$, η is the viscosity, k_B Boltzmann constant and T temperature, D_i is the diffusion coefficient of ith solute and z_i its valency if

charged. These equations together with the inhomogeneous boundary conditions (BC) on the surface of the Janus sphere and as $\bar{r}\to\infty$ (see next section) define a boundary value problem whose approximate solution is the subject of this paper.

We consider the system in the steady state (time derivatives equal to zero), the dynamics of the fluid around the swimmer in the zero Reynolds number ($Re=0$) limit of the Navier–Stokes equations for incompressible fluid flow. In this paper we restrict ourselves to zero Peclét number, equivalent to assuming that diffusion of the solutes occurs much faster than their convection by the flows generated by the Janus particle – very reasonable for the experimental systems we attempt to describe. Thus, the fluid velocity given by $\bar{\boldsymbol{v}}(\bar{\boldsymbol{r}}) = \bar{v}_r\hat{\boldsymbol{e}}_{\bar{r}} + \bar{v}_\theta\hat{\boldsymbol{e}}_\theta$ obeys the Stokes equation, while the solute concentration fields $\bar{c}_q, \bar{c}_n$ are governed by the steady-state drift-diffusion equations.

$$0 = \bar{\boldsymbol{\nabla}}\cdot\bar{\boldsymbol{v}}, \tag{2.5}$$

$$\mathbf{0} = \boldsymbol{\nabla}\cdot\bar{\boldsymbol{\Pi}} + \bar{\boldsymbol{f}} = \eta\bar{\nabla}^2\bar{\boldsymbol{v}} - \bar{\boldsymbol{\nabla}}\bar{p} - \sum_{i\in ions} ez_i\bar{c}_i\bar{\boldsymbol{\nabla}}\bar{\Phi} - \sum_{j\in non\text{-}ions}\bar{c}_j\bar{\boldsymbol{\nabla}}\bar{\Psi}_j, \tag{2.6}$$

$$0 = -\bar{\boldsymbol{\nabla}}\cdot\bar{\boldsymbol{J}}_q; \quad \bar{\boldsymbol{J}}_q = -D_q\bar{\boldsymbol{\nabla}}\bar{c}_q - \frac{D_q z_q e\bar{c}_q}{k_BT}\bar{\boldsymbol{\nabla}}\bar{\Phi}; \quad q\in \text{ions}, \tag{2.7}$$

$$0 = -\bar{\boldsymbol{\nabla}}\cdot\bar{\boldsymbol{J}}_n; \quad \bar{\boldsymbol{J}}_n = -D_n\bar{\boldsymbol{\nabla}}\bar{c}_n - \frac{D_n\bar{c}_n}{k_BT}\bar{\boldsymbol{\nabla}}\bar{\Psi}_n; \quad n\in \text{non-ions}, \tag{2.8}$$

where we have defined $\bar{\boldsymbol{\Pi}}(\bar{\boldsymbol{r}}) = \eta(\boldsymbol{\nabla}\boldsymbol{v} + \boldsymbol{\nabla}\boldsymbol{v}^{\mathrm{T}}) - p\boldsymbol{\delta}$, the local hydrodynamic stress tensor.

2.2. *Boundary conditions*

The hydroxide and the salt ions are not involved directly in the catalytic decomposition of the fuel (1.1) so we impose zero flux boundary conditions for their concentrations on the surface of the Janus particle,

$$\hat{\boldsymbol{n}}\cdot\bar{\boldsymbol{J}}_{oh}|_{\bar{r}=a} = 0 = \hat{\boldsymbol{n}}\cdot\bar{\boldsymbol{J}}_{s,\pm}|_{\bar{r}=a}, \tag{2.9}$$

where the unit vector, $\hat{\boldsymbol{n}} = (\sin\theta\cos\phi, \sin\theta\sin\phi, \cos\theta) = \hat{\boldsymbol{e}}_r$ in spherical polar coordinates. We define a catalyst coverage function, $K(\cos\theta)$ which is 1 on the platinum hemisphere and zero on the polystyrene hemisphere,

$$K(\cos\theta) = \begin{cases} 1, & 0\leqslant\cos\theta\leqslant 1 \\ 0, & -1\leqslant\cos\theta < 0. \end{cases} \tag{2.10}$$

The presence of protons as intermediates of the fuel decomposition reaction (1.1) and the variation of the reaction rates across the Pt-coated hemisphere leads to non-zero flux boundary conditions for the proton concentration on the surface of the Janus sphere

$$\hat{\boldsymbol{n}}\cdot\bar{\boldsymbol{J}}_h|_{\bar{r}=a} = \bar{\mathcal{J}}_h(\theta)K(\cos\theta), \tag{2.11}$$

where the proton current, $\bar{\mathcal{J}}_h$, varies with θ (position along the Pt-coated hemisphere). The specific form of the proton current $\bar{\mathcal{J}}_h$ will depend on the details of the reaction kinetics (see § 2.4 and appendix A). However, we note that $\bar{\mathcal{J}}_h > 0$ implies a chemical reaction producing protons while $\bar{\mathcal{J}}_h < 0$ implies a proton sink.

The fuel decomposition reaction involves the neutral species, H_2O_2 and O_2 giving rise to non-zero flux boundary conditions for their concentrations on the Janus particle surface,

$$\hat{\boldsymbol{n}} \cdot \bar{\boldsymbol{J}}_o|_{\bar{r}=a} = \bar{\mathcal{J}}_o(\theta) K(\cos\theta), \tag{2.12}$$

$$\hat{\boldsymbol{n}} \cdot \bar{\boldsymbol{J}}_{hp}|_{\bar{r}=a} = \bar{\mathcal{J}}_{hp}(\theta) K(\cos\theta), \tag{2.13}$$

where $\bar{\mathcal{J}}_{hp}(\theta) < 0$ indicates H_2O_2 decomposition while $\bar{\mathcal{J}}_o(\theta) > 0$ indicates production of the O_2. Because of the variations in thickness of the Pt-coating, both $\bar{\mathcal{J}}_{hp}(\theta)$, $\bar{\mathcal{J}}_o(\theta)$, defined in appendix A, are functions of position along the Pt-coated hemisphere.

All the concentrations, $\bar{c}_i(\bar{\boldsymbol{r}})$, decay to their background values, $\bar{c}_i^{\infty}$ as $\bar{r} \to \infty$.

We have Dirichlet boundary conditions for the electric potential on the particle surface

$$\bar{\Phi}(\bar{r} = a) = \bar{\varphi}_s(\theta), \tag{2.14}$$

where $\bar{\varphi}_s$ is a possibly varying function over the swimmer surface. The potential, $\bar{\varphi}_s$ will in general be pH dependent and will also depend on the particular reaction scheme of catalytic fuel decomposition. For our analysis, it is sufficient to know the average value $\langle\bar{\varphi}_s\rangle = (1/2\pi) \int \mathrm{d}\cos\theta\, \bar{\varphi}_s(\theta)$ and in the following we take $\bar{\varphi}_s \equiv \langle\bar{\varphi}_s\rangle$. The potential $\bar{\varphi}_s$ can be related to the swimmer surface charge by double-layer models (Russel, Saville & Schowalter 1992).

The boundary conditions for the fluid velocity field are

$$\bar{\boldsymbol{v}}|_{\bar{r}=a} = \bar{\boldsymbol{U}} + \bar{\boldsymbol{\Omega}} \times \bar{\boldsymbol{r}}; \quad \bar{\boldsymbol{v}}(\bar{r} \to \infty) = \boldsymbol{0}, \tag{2.15a,b}$$

where $\bar{\boldsymbol{U}}$, $\bar{\boldsymbol{\Omega}}$ are respectively the total linear and angular propulsion velocities of the swimmer. These are unknown and their calculation is the goal of this paper.

2.3. *Constraints*

(Quasi-steady state condition) As we study the system in a quasi-steady state, this requires that the average proton current on the swimmer surface vanishes,

$$\oint_{\bar{r}=a} \bar{\mathcal{J}}_h(\theta) K(\cos\theta) \sin\theta \, \mathrm{d}\theta = 0, \tag{2.16}$$

and note that this also guarantees conservation of the surface charge (Moran & Posner 2011).

(Swimming conditions) We consider a freely swimming Janus particle with no external load on the colloid which requires that there is zero total force and torque on the swimmer:

$$\bar{\boldsymbol{F}} = \oint_{\bar{r}=a} \bar{\boldsymbol{\Pi}} \cdot \hat{\boldsymbol{n}} \, \mathrm{d}\mathcal{S}_p + \int \bar{\boldsymbol{f}} \, \mathrm{d}\mathcal{V}_p = \boldsymbol{0}, \tag{2.17}$$

$$\bar{\boldsymbol{T}} = \oint_{\bar{r}=a} \bar{\boldsymbol{r}} \times \left(\bar{\boldsymbol{\Pi}} \cdot \hat{\boldsymbol{n}}\right) \mathrm{d}\mathcal{S}_p + \int \bar{\boldsymbol{r}} \times \bar{\boldsymbol{f}} \, \mathrm{d}\mathcal{V}_p = \boldsymbol{0}, \tag{2.18}$$

where $\mathrm{d}\mathcal{S}_p$ ($\mathrm{d}\mathcal{V}_p$) is the differential surface (volume) element. These two conditions uniquely determine both propulsion velocities ($\bar{\boldsymbol{U}}$, $\bar{\boldsymbol{\Omega}}$) (Anderson 1989).

The linearity of the Stokes equation and the limit of vanishing Peclét number, mean that we can divide the linear and angular velocities into non-electric, i.e.

neutral diffusiophoretic, (due to the terms on the right-hand side of (2.6) depending on the $\bar{\Psi}_j$), and electric, i.e. ionic-diffusiophoretic and electrophoretic, contributions (due to the terms on the right-hand side of (2.6) depending on $\bar{\Phi}$), which can each be calculated separately,

$$\bar{\boldsymbol{U}} = \bar{\boldsymbol{U}}^e + \bar{\boldsymbol{U}}^d, \tag{2.19}$$

$$\bar{\boldsymbol{\Omega}} = \bar{\boldsymbol{\Omega}}^e + \bar{\boldsymbol{\Omega}}^d, \tag{2.20}$$

where $(\bar{\boldsymbol{U}}^e, \bar{\boldsymbol{\Omega}}^e)$ are electric and $(\bar{\boldsymbol{U}}^d, \bar{\boldsymbol{\Omega}}^d)$ are non-electric. We expect (and indeed find) that the neutral-diffusiophoretic contribution to the propulsion is much smaller than the electrophoretic contribution. While we will later briefly outline the calculation of the neutral-diffusiophoretic contribution to the propulsion velocity in § 3.2, in this article we will focus on the electrophoretic and ionic-diffusiophoretic contributions. Detailed calculations of the neutral-diffusiophoretic contribution can be found in the literature (Anderson, Lowell & Prieve 1982; Golestanian *et al.* 2005, 2007; Michelin & Lauga 2014).

Due to the axisymmetry of the swimmer and the constraint of zero torque (2.18), the angular velocity ($\bar{\boldsymbol{\Omega}}$) vanishes identically ($\bar{\boldsymbol{\Omega}}^e = \boldsymbol{0}$, $\bar{\boldsymbol{\Omega}}^d = \boldsymbol{0}$). Therefore in the following we will only consider the swimmer velocity $\bar{\boldsymbol{U}}$.

2.4. *Dependence of reaction rate constants on Pt-coating thickness*

The cornerstone of our analysis in this paper is the identification of the fact that the reaction rate of H_2O_2 decomposition depends on the Pt-coating thickness (Ebbens *et al.* 2014). A further observation is the well-known presence of additional chemical pathways in the decomposition which involve charged intermediates, in particular protons, (Hall *et al.* 1998, 1999*a*,*b*). These charged intermediates, in conjunction with the variation of Pt-coating thickness, allow an electric current to be established in the Pt shell due to varying decomposition rates of the hydrogen peroxide on different parts of the shell. We approximate for simplicity that this thickness variation is linear in $\cos\theta$, with a peak at the pole and the minimum at the equator,

$$k_i(\theta) = k_i^{(0)} + \sum_l k_i^{(l)} P_l(\cos\theta) \simeq k_i^{(0)} + k_i^{(1)} \cos\theta, \tag{2.21}$$

where $k_i(\theta)$ is the reaction rate 'constant' for the ith reaction step in reaction (1.1) above and $P_n(x)$ is the Legendre polynomial of order n. The Legendre moments $k_i^{(l)} = (l+1/2)\int_{-1}^{1} k_i(\theta) P_l(\cos\theta)\,\mathrm{d}\cos\theta$. We assume weak variation ($k_i^{(1)} \ll k_i^{(0)}$) allowing us to work perturbatively in the variation. As long as there is a competition between a neutral pathway and a pathway involving charged intermediates, conservation of charge in the steady state requires that the varying reaction rates across the Pt-coating lead to establishment of electric currents in the Pt shell. This is described in detail for a particular reaction scheme involving protons in appendix A, however the qualitative features of our results do not depend on the details of the scheme.

3. Analysis

Guided by current experiments, we analyse the coupled problem of the concentrations, electrostatic potential and fluid flow by considering situations in which the length scale of the interactions (Debye screening length, κ^{-1} for charged

species and effective interaction range L_{eff} for the neutral species) is small compared to the size (radius $=a$) of the swimmer. We verify *a posteriori* that this is indeed the case. The effective diffusiophoretic interaction range L_{eff} for all the neutral solutes is defined as $L_{eff}^2 = (\eta/k_BT)\bar{\mu}_d^{\ddagger}$, where $\bar{\mu}_d^{\ddagger} = (k_BT/\eta)\int_0^\infty \rho(1 - e^{-\bar{\Psi}/k_BT})\,\mathrm{d}\rho > 0$ is the characteristic diffusiophoretic mobility of the Janus particle. Hence the problem can naturally be viewed as one with two very separate length scales with small parameters $\lambda = 1/(\kappa a)$, $\chi = L_{eff}/a$ for charged and neutral species respectively. A robust bound for comparison with experiment would be $\lambda \leqslant 0.1$. A useful approach to multi-scale problems with a small parameter multiplying the differential operator of highest order, is the decomposition of the domain of the solution into a boundary layer, where the fields vary on the small $O(\lambda)$ length scale ($O(\chi)$ for the diffusiophoretic contribution) and an outer domain where the characteristic length scale is the size of the swimmer 'a'. To do this most efficiently, we group the dimensional quantities into useful dimensionless groups whose variation determines the behaviour of the system.

3.1. *Self-electrophoresis and ionic self-diffusiophoresis*

In this section, we describe detailed calculations of the electrophoretic and ionic-diffusiophoretic contributions to the swimming velocity which is the main focus of the paper.

3.1.1. *Dimensionless equations*

We non-dimensionalize the equations as follows. The position vector $\bar{\boldsymbol{r}}$ is measured in units of the swimmer size 'a', concentrations $\bar{c}_i$ in units of the steady-state background values c_i^∞, electric potential $\bar{\Phi}$ in terms of the thermal voltage $(e\beta)^{-1}$ (with $\beta^{-1} = k_BT$, k_B Boltzmann constant and T temperature), ionic solute fluxes, $\bar{\boldsymbol{J}}_q$ in terms of $D_q\sum_i |z_i|^2 c_i^\infty/a$, with D_i the diffusion coefficient of ith solute and z_i its valency. The fluid flow velocity $\bar{\boldsymbol{v}}$ is rescaled by $\epsilon/(e^2\beta^2\eta a)$, while the pressure $\bar{p}$ is rescaled by $\epsilon/(e^2\beta^2a^2)$. Hence we express dimensionless quantities (without overbar) in terms of the dimensional (with overbar): $\boldsymbol{r} = (x, y, z) = \bar{\boldsymbol{r}}/a$, $c_i = \bar{c}_i/c_i^\infty$, $\Phi = e\beta\bar{\Phi}$, $\boldsymbol{v} = \bar{\boldsymbol{v}}e^2\beta^2\eta a/\epsilon$, $p = \bar{p}e^2\beta^2 a/\epsilon$.

It is useful for us to define the dimensionless deviations of the solute concentrations, $C_i(\boldsymbol{r}) \equiv c_i(\boldsymbol{r}) - 1 = (\bar{c}_i/c_i^\infty) - 1$ from their bulk values. Hence we obtain the following dimensionless equations of motion:

(i) The steady-state equations for concentration differences of the charged species; protons C_h, hydroxide ions C_{oh} and the salt $C_{s\pm}$,

$$\boldsymbol{\nabla}\cdot\boldsymbol{J}_i = 0; \quad \boldsymbol{J}_i = -\boldsymbol{\nabla}C_i - z_i(1 + C_i)\boldsymbol{\nabla}\Phi, \tag{3.1a,b}$$

where $i \in \{h, oh, s\pm\}$. We consider only monovalent salts $|z_i| = 1$.

(ii) The dimensionless Poisson equation for the electric potential $\Phi(\boldsymbol{r})$,

$$-\lambda^2\nabla^2\Phi = \sum_{i\in\{h,oh,s\pm\}} \mathcal{Z}_i C_i. \tag{3.2}$$

(iii) The dimensionless Stokes equations for the fluid velocity $\boldsymbol{v}(\boldsymbol{r})$,

$$0 = \boldsymbol{\nabla}\cdot\boldsymbol{v}, \tag{3.3}$$

$$\boldsymbol{0} = \boldsymbol{\nabla}\cdot\boldsymbol{\Sigma} = \nabla^2\boldsymbol{v} - \boldsymbol{\nabla}p - \lambda^{-2}\sum_{i\in\,ions} \mathcal{Z}_i C_i\boldsymbol{\nabla}\Phi, \tag{3.4}$$

where the dimensionless parameters λ and $\mathcal{Z}_i$ are defined as

$$\lambda^2 \equiv (\kappa a)^{-2}; \quad \kappa^{-2} = \frac{\epsilon k_B T}{e^2 \sum_j |z_j|^2 c_j^\infty} = \frac{1}{4\pi l_B \sum_j |z_j|^2 c_j^\infty}; \quad \mathcal{Z}_i = \frac{z_i c_i^\infty}{\sum_j |z_j|^2 c_j^\infty}, \quad (3.5a\text{–}c)$$

where ϵ is the permittivity of the solvent and e is the electronic charge. κ^{-1} is the Debye screening length and $l_B = e^2/4\pi\epsilon k_B T$ is the Bjerrum length (Russel *et al.* 1992). We note that the stress $\boldsymbol{\Sigma}$ is the sum of the hydrodynamic stress tensor and the Maxwell stress tensor due to the interactions of the charged species with each other and the colloid surface.

The zero total force condition which determines the propulsion velocity $\boldsymbol{U}^e$ becomes

$$\boldsymbol{F} = \oint_{r=1} \boldsymbol{\Sigma} \cdot \hat{\boldsymbol{n}} \sin\theta \, \mathrm{d}\theta = \boldsymbol{0}. \quad (3.6)$$

3.1.2. *Dimensionless boundary conditions*

For the electric potential on the swimmer surface,

$$\Phi(r=1) = \varphi_s, \quad (3.7)$$

and decays to zero in the bulk far from the swimmer, $\Phi(r \to \infty) = 0$.

For the flow field on the swimmer surface,

$$\boldsymbol{v}|_{r=1} = \boldsymbol{U}^e, \quad (3.8)$$

and $\boldsymbol{v}(r \to \infty) = \boldsymbol{0}$ far in the bulk, where $\boldsymbol{U}^e$ is the electric contribution to the propulsion velocity.

For the hydroxide and the salt concentrations, the zero flux boundary conditions due to the impermeability of the Janus particle surface,

$$\hat{\boldsymbol{n}} \cdot \boldsymbol{J}_{oh}|_{r=1} = 0 = \hat{\boldsymbol{n}} \cdot \boldsymbol{J}_{s,\pm}|_{r=1}. \quad (3.9)$$

For the proton concentration, the non-zero flux boundary condition,

$$\hat{\boldsymbol{n}} \cdot \boldsymbol{J}_h|_{r=1} = \mathcal{J}_h(\theta) K(\cos\theta). \quad (3.10)$$

The essential mechanism which drives this process depends on the presence of a (i) varying proton flux (as a result of variation of Pt thickness) which (ii) averages to zero over the metallic hemisphere (due to charge conservation in the steady state). In the limit of small linear variation in the thickness, this leads to a proton flux of the general form

$$\mathcal{J}_h(\theta) = \gamma^{(1)} (1 - 2\cos\theta) K(\cos\theta) - \gamma^{(0)} \delta (\Phi + C_h) K(\cos\theta), \quad (3.11)$$

where both $\gamma^{(i)} \neq 0$. We note that $\gamma^{(1)} = 0$ for a uniform thickness coating and $\delta(\Phi + C_h) = [(\Phi + C_h) - \int_0^\pi (\Phi + C_h) K(\cos\theta) \sin\theta \, \mathrm{d}\theta]$ is the deviation of the local electric field and proton concentration from their surface average. $\gamma^{(0)}$ is a measure of the scale of typical production and consumption of protons across the metallic hemisphere. Since both terms on the right-hand side of (3.11) integrated over the surface give zero, the flux, $\mathcal{J}_h$ automatically satisfies the steady-state requirement (2.16) and hence the conservation of total charge on the swimmer surface.

Systems which possess both properties above, with both $\gamma^{(i)} > 0$, will show all the qualitative behaviours described in this article, however their values will depend on the specific details of the chemical reaction scheme. A specific reaction scheme described

in detail in appendix A gives:

$$\gamma^{(0)} = \frac{k_{eff}^{(h)} c_{hp}^{\infty} a}{D_h \sum_i c_i^{\infty}}; \quad \gamma^{(1)} = \frac{\Delta k_{eff}^{(h)} c_{hp}^{\infty} a}{D_h \sum_i c_i^{\infty}}, \tag{3.12a,b}$$

where $k_{eff}^{(h)} > 0$ is the typical scale of the average proton consumption and production while $\Delta k_{eff}^{(h)} > 0$ is the scale of the difference between the rates at the pole and equator (see appendix A for their derivation from reaction kinetics).

We note that the conservation of protons also requires a relationship between the pH of the solution and the potential on the surface of the Janus particle, which depends on the reaction kinetics (see appendix A);

$$\varphi_s = \varphi_s(c_h^{\infty}), \tag{3.13}$$

leading to an estimate of the average swimmer surface charge ($\sigma_0(c_h^{\infty})$) using the Gouy–Chapman model (Russel *et al.* 1992) of the interfacial double layer

$$\sigma_0(c_h^{\infty}) = \frac{e\kappa}{2\pi l_B} \sinh\left(\frac{\varphi_s}{2}\right), \tag{3.14}$$

where $l_B = e^2/4\pi\epsilon k_B T$ is the Bjerrum length, with ϵ the solution permittivity.

In this electrostatic problem, the inner boundary layer (double layer) fields, $H(\boldsymbol{r}) \in \{c_i(\boldsymbol{r}), \boldsymbol{v}(\boldsymbol{r}), \boldsymbol{\Phi}(\boldsymbol{r})\}$ are expanded as

$$H(r,\theta) = \sum_n \lambda^n \mathcal{H}^{(n)}(\rho,\theta); \quad \rho = \frac{r-1}{\lambda}, \tag{3.15a,b}$$

while the outer fields, $H(\boldsymbol{r}) \in \{c_i(\boldsymbol{r}), \boldsymbol{v}(\boldsymbol{r}), \boldsymbol{\Phi}(\boldsymbol{r})\}$ are expanded as

$$H(r,\theta) = H^{(0)}(r,\theta) + \sum_{n=1}^{\infty} \lambda^n H^{(n)}(r,\theta), \tag{3.16}$$

where r is the bulk-scale coordinate. Similar expansions will apply for the self-diffusiophoretic problem, with λ replaced by χ.

The essence of the matched asymptotic method involves obtaining asymptotic expansions of the solutions of the equations in the limit $\lambda \to 0$ for both the inner and outer fields and matching the results in the intermediate region:

$$\lim_{\lambda\to 0;\rho\to\infty} \{\mathcal{H}_i^{(0)}\}(\rho,\theta) = \lim_{r\to 1;\lambda\to 0} \{H_i^{(0)}\}(r,\theta) = \{H_i\}(1,\theta). \tag{3.17}$$

In the next section, we will proceed to solve the outer problem in the limit of $\lambda = (\kappa a)^{-1} \to 0$, i.e. thin double-layer limit where the swimmer radius a is much larger than the Debye-layer thickness κ^{-1}. The details of the inner (Debye-layer) calculations (Prieve *et al.* 1984; Yariv 2011) can be found in the appendix B (see figure 3).

3.1.3. *Outer concentration and electric fields*

In the bulk, the fields vary over length scales comparable to the swimmer size, with $O(1)$ leading-order fields, and are expanded as

$$H(r,\theta) = H^{(0)}(r,\theta) + \lambda H^{(1)}(r,\theta) + \cdots. \tag{3.18}$$

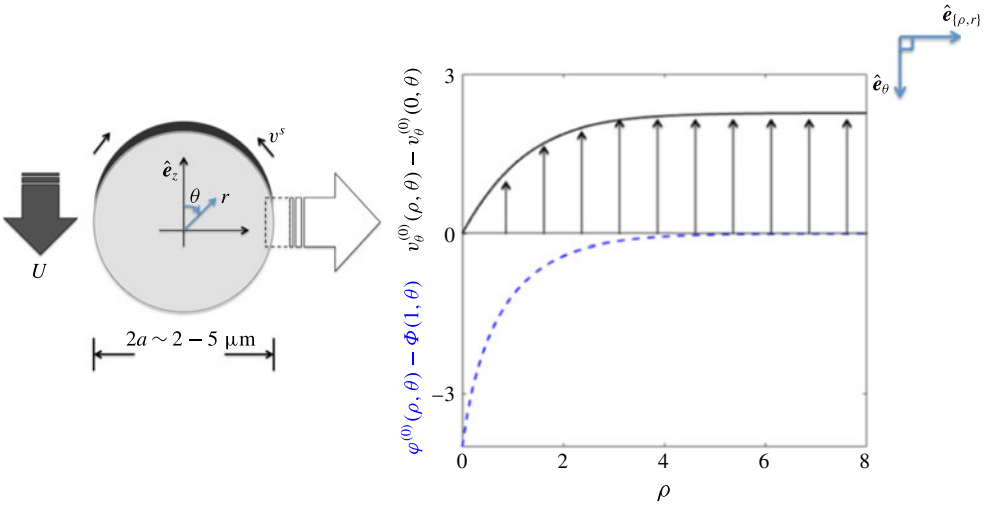

FIGURE 3. (Colour online) Profiles of flow and electric field within the (inner) Debye layer with $C_s^* = \partial C_s^*/\partial\theta = \partial\Phi/\partial\theta = 1$ (see appendix B).

We drop the $^{(0)}$ superscript in the following as we will consider only the leading-order terms $C^{(0)}$, $\Phi^{(0)}$, $v_i^{(0)}$, $p^{(0)}$, in the expansions for the fields.

The leading-order solute concentrations and electric potential outside the Debye layer obey the equations

$$\sum_{i\in\{h,oh,s\pm\}} \mathcal{Z}_i C_i = 0, \tag{3.19}$$

$$\boldsymbol{\nabla}\cdot[\boldsymbol{\nabla}C_i + z_i(1+C_i)\boldsymbol{\nabla}\Phi] = 0, \tag{3.20}$$

where $\mathcal{Z}_i$ is defined in (3.5). It is useful for the rest of our analysis to treat all the ionic solutes together. Combining the two equations (3.19) and (3.20), we obtain,

$$\nabla^2 C^* = 0, \tag{3.21}$$

$$\boldsymbol{\nabla}\cdot(C^*\boldsymbol{\nabla}\Phi) = 0, \tag{3.22}$$

where we have defined the sum of the deviations of concentration of all of the ionic solutes and its value at $r = 1$.

$$C^*(r,\theta) = 2\sum_{i\in\{h,s+\}} \mathcal{Z}_i\,(1 + C_i(r,\theta)); \tag{3.23}$$

$$C_s^*(\theta) \equiv C^*(r=1,\theta). \tag{3.24}$$

The boundary conditions for Φ and C^* are obtained by matching to the inner solutions (see appendix B), giving

$$-\hat{\boldsymbol{n}}\cdot\boldsymbol{\nabla}C^*|_{r=1} = \gamma^{(1)}\,(1-2\cos\theta)\,K(\cos\theta) - \gamma^{(0)}\delta(\Phi + C_h)K(\cos\theta), \tag{3.25}$$

$$-\hat{\boldsymbol{n}}\cdot(C^*\boldsymbol{\nabla}\Phi|_{r=1} = \gamma^{(1)}\,(1-2\cos\theta)\,K(\cos\theta) - \gamma^{(0)}\delta\,(\Phi + C_h)\,K(\cos\theta), \tag{3.26}$$

from equations (3.10) and (3.11).

The fluid velocity field in the outer region obeys the equation

$$\nabla^2 \boldsymbol{v} - \boldsymbol{\nabla} p + \nabla^2 \Phi \boldsymbol{\nabla} \Phi = \boldsymbol{0}, \tag{3.27}$$

with the slip boundary condition (Prieve *et al.* 1984)

$$\boldsymbol{v}(1, \theta) = \boldsymbol{U}^e + \left[\zeta(\theta) \frac{\partial \Phi}{\partial \theta} + 4 \ln \cosh \left(\frac{\zeta(\theta)}{4} \right) \frac{\partial \ln C_s^*}{\partial \theta} \right] \hat{\boldsymbol{e}}_\theta, \tag{3.28}$$

and quiescent fluid far away from the swimmer, $\boldsymbol{v} \to \boldsymbol{0}$ as $r \to \infty$. The slip boundary condition for $\boldsymbol{v}$ is obtained by matching to the inner solution (see appendix B).

3.1.4. *Linear response and propulsion velocity*

We note that with uniform coating, $k_i = k_i^{(0)}$, which implies $\gamma^{(1)} = 0$, the deviations of the electric potential and the ionic concentrations vanish ($\Phi = 0 = C_i$). The ζ potential for this trivial solution is

$$\zeta_0 := \zeta = \varphi_s. \tag{3.29}$$

In addition, this implies the fluid velocity field vanishes $\boldsymbol{v} = \boldsymbol{0}$, and hence the contribution of self-electrophoresis to the propulsion velocity vanishes $\boldsymbol{U}^e = \boldsymbol{0}$. However, a varying thickness coating and the consequent non-zero $\gamma^{(1)}$, lead to a qualitatively different scenario. To explore this we perform an expansion to linear order in $\gamma^{(1)}/\gamma^{(0)}$ of the fields for the concentrations, fluid velocity, pressure and electric potential: $\{C_i, \boldsymbol{v}, p, \Phi\}$ for $\gamma^{(1)} \ll \gamma^{(0)}$, where $\gamma^{(1)}, \gamma^{(0)}$ are defined in (3.12).

We first expand the deviations of the concentrations and the electric field as

$$H = \gamma^{(1)} H^{(\gamma)} + O((\gamma^{(1)})^2), \tag{3.30}$$

with $H \in \{C_i, C^*, \Phi\}$ and keeping only linear terms. Substituting these perturbative fields into (3.21), (3.22), we find that at leading order, $C^{*(\gamma)}$ decouples from the electric potential field $\Phi^{(\gamma)}$ – with both obeying Laplace equations

$$\nabla^2 C^{*(\gamma)} = 0, \tag{3.31}$$

$$\nabla^2 \Phi^{(\gamma)} = 0, \tag{3.32}$$

and the boundary conditions, from the matching with the inner solution, at this order are

$$-\hat{\boldsymbol{n}} \cdot \boldsymbol{\nabla} C^{*(\gamma)}\big|_{r=1} = -\hat{\boldsymbol{n}} \cdot \boldsymbol{\nabla} \Phi^{(\gamma)}\big|_{r=1} = (1 - 2x)\, K(x) - \gamma^{(0)} \delta(\Phi^{(\gamma)} + {C_h}^{(\gamma)}) K(x), \tag{3.33}$$

where $x = \cos\theta$, $\delta(\Phi^{(\gamma)} + {C_h}^{(\gamma)}) = [(\Phi^{(\gamma)} + {C_h}^{(\gamma)}) - \int_0^1 (\Phi^{(\gamma)} + {C_h}^{(\gamma)})\, \mathrm{d}x]$.

Now, the Laplace equations above for $C^{*(\gamma)}$, $\Phi^{(\gamma)}$ in conjunction with the electroneutrality condition (3.19) imply (see figure 4)

$$\Phi^{(\gamma)}(r, \theta) = {C_h}^{(\gamma)}(r, \theta) = C^{*(\gamma)}(r, \theta) - 1 = \sum_{l=0}^{\infty} A_l r^{-(l+1)} P_l(\cos\theta), \tag{3.34}$$

where $P_l(\cos\theta)$ are the Legendre polynomials. The unknown coefficients A_l are determined by the boundary conditions in (3.33) above.

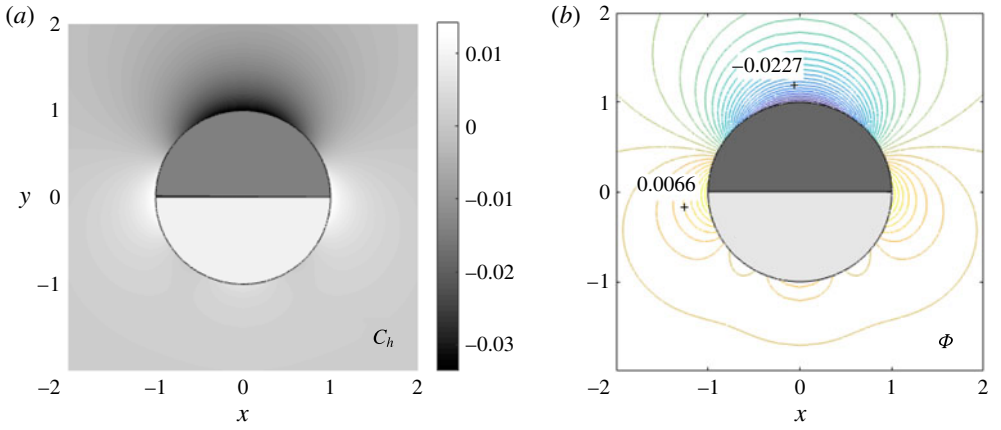

FIGURE 4. (Colour online) (*a*) Proton concentration deviation from the uniform background profile and (*b*) associated electric potential difference contours (both plots with pH = 5.5 for 10 % H_2O_2 without salt and the system parameters in table 1). The equipotential contours 0.0066 and −0.0227 (in units of the thermal voltage (k_BT/e) ≈ 25 mV) are shown to indicate the electric pole–equator polarity. In both panels, the upper (dark) hemisphere is the platinum cap.

Description	Symbol	Value	Units (SI)
Boltzmann energy scale (at 300 K)	k_BT	4.05×10^{-21}	J
Permittivity (water)	ϵ	6.90×10^{-10}	$CV^{-1}\ m^{-1}$
Electronic charge	e	1.60×10^{-19}	C
Average surface charge density (at zero salt conc.)	σ_0	1.60×10^{-3}	Cm^{-2}
Viscosity of water (at 300 K)	η	8.9×10^{-4}	$Nm^{-2}\ s^{-1}$
Diffusiophoretic characteristic mobility	$\bar{\mu}_d^{\ddagger}$	4.57×10^{-38}	$m^5\ s^{-1}$
Peroxide [H_2O_2] diffusion coefficient	D_{hp}	6.60×10^{-10}	$m^2\ s^{-1}$
Oxygen [O_2] diffusion coefficient	D_o	2.00×10^{-9}	$m^2\ s^{-1}$
Protons [H^+] diffusion coefficient	D_h	9.30×10^{-9}	$m^2\ s^{-1}$
Swimmer radius	a	1.00×10^{-6}	m
H_2O_2 decomposition reaction rate ($\mathcal{K} := k_{eff}^{(hp)} c_{hp}^{\infty}$) (Brown & Poon 2014; Ebbens *et al.* 2014)	$\mathcal{K}$	3.00×10^{22}	$m^{-2}\ s^{-1}$
10 % w/v H_2O_2 number concentration	c_{hp}^{∞}	1.76×10^{27}	m^{-3}
Effective proton absorption/release rate (∼0.3 %$\mathcal{K}$)	$k_{eff}^{(h)} c_{hp}^{\infty}$	1.00×10^{20}	$m^{-2}\ s^{-1}$
Proton pole-to-equator rate 'difference' (∼0.09 %$\mathcal{K}$)	$\Delta k_{eff}^{(h)} c_{hp}^{\infty}$	2.70×10^{19}	$m^{-2}\ s^{-1}$

TABLE 1. System parameters.

Finally, the coefficients A_l are obtained as a self-consistent system of equations,

$$\sum_{l=0}^{\infty} A_l (l+1) P_l(x) = (1-2x)K(x) - 2\gamma^{(0)} \sum_{l=0}^{\infty} A_l \left(P_l(x) - \int_0^1 P_l(x')\,\mathrm{d}x' \right) K(x), \quad (3.35)$$

where $x = \cos\theta$.

Using the orthogonality of the Legendre polynomials, we obtain a linear system of equations for the coefficients A_l,

$$\begin{pmatrix} 1 & 0 & 0 & \cdots & 0 & \cdots \\ 0 & M_{11} & M_{12} & \cdots & M_{1l} & \cdots \\ 0 & M_{21} & M_{22} & \cdots & M_{2l} & \cdots \\ \vdots & \vdots & \vdots & \ddots & \vdots & \cdots \\ 0 & M_{n1} & M_{n2} & \cdots & M_{nl} & \cdots \\ \vdots & \vdots & \vdots & \vdots & \vdots & \ddots \end{pmatrix} \begin{pmatrix} A_0 \\ A_1 \\ A_2 \\ \vdots \\ A_l \\ \vdots \end{pmatrix} = \begin{pmatrix} 0 \\ \Lambda_1 \\ \Lambda_2 \\ \vdots \\ \Lambda_n \\ \vdots \end{pmatrix} \tag{3.36}$$

or more compactly

$$\boldsymbol{M} \cdot \boldsymbol{A} = \boldsymbol{\Lambda}, \tag{3.37}$$

where $\boldsymbol{A} = (A_0, \ldots, A_N, \ldots)$, and the matrix $\boldsymbol{M}$ and vector $\boldsymbol{\Lambda}$ entries are given by

$$M_{nl} = \delta_{nl} + \gamma^{(0)} \left(\frac{2n+1}{n+1} \right) \int_0^1 P_n(x) \left(P_l(x) - \int_0^1 P_l(x')\, \mathrm{d}x' \right) \mathrm{d}x, \tag{3.38}$$

$$\Lambda_n = \frac{1}{2} \left(\frac{2n+1}{n+1} \right) \int_0^1 (1-2x)\, P_n(x)\, \mathrm{d}x. \tag{3.39}$$

The infinite linear system of equations (3.36) above can be solved approximately by truncating the infinite system after a finite number of components, reducing the description to the first N Legendre coefficients A_l. The approximate (numerical) solution requires inversion of an $N \times N$ matrix $\boldsymbol{M}$ (see figure 5). However, we can extract asymptotic regimes of this solution for $\gamma^{(0)} \ll 1$ and $\gamma^{(0)} \gg 1$. Note that $\gamma^{(1)} \ll \gamma^{(0)}$ in both limits.

$\gamma^{(0)} \ll 1$: In this regime, $A_l \sim \Lambda_l$ and

$$A_1 \sim -\tfrac{1}{8} \tag{3.40}$$

$\gamma^{(0)} \gg 1$: In this regime,

$$A_1 \sim -\frac{\alpha}{\gamma^{(0)}}, \tag{3.41}$$

where α is a positive constant whose value can be determined numerically. The asymptotes show that the perturbations of C_i and Φ decay to zero for large $\gamma^{(0)}$ (proportional to swimmer size) – when the diffusion time becomes large compared to the reaction time.

In figure 5(*a*), the deviations of the proton concentration ${C_h}^{(\gamma)}(1, \theta)$ and electric potential $\Phi^{(\gamma)}(1, \theta)$ on the surface from their bulk values are plotted showing the an excess at the equator and depletion at the pole. Increasing the number of Legendre polynomial modes (N) improves the accuracy of the fields on the polystyrene hemisphere. The proton depletion (excess) at the pole (equator) is stronger for larger swimmer sizes (see figure 5*b*).

The calculated coefficients A_l above determine the slip velocity and we can now solve the Stokes flow problem. Hence, as above, we expand the velocity and pressure fields about the trivial solution $\boldsymbol{v} = \boldsymbol{0}, p = p_\infty$,

$$\boldsymbol{v} = \gamma^{(1)} \boldsymbol{v}^{(\gamma)} + \cdots; \tag{3.42}$$

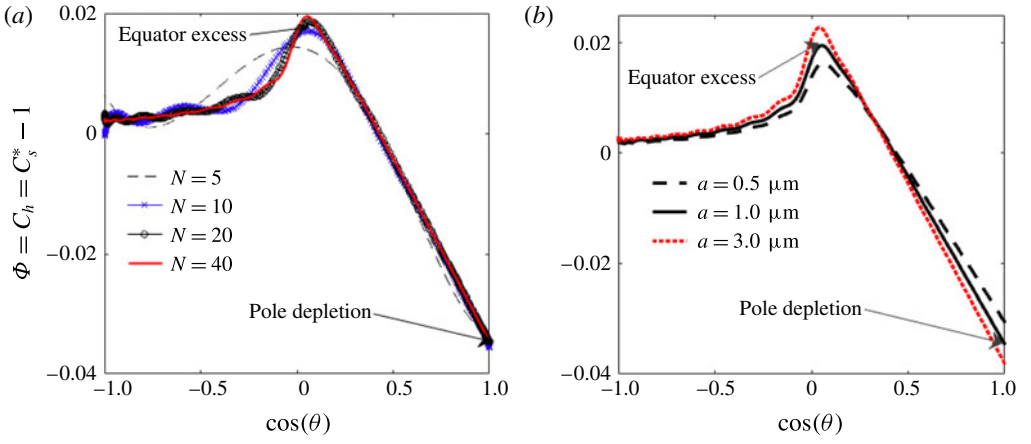

FIGURE 5. (Colour online) (*a*) The deviations of the surface electric potential, $\Phi(1,\theta)$, and ionic concentrations, $C_h(1,\theta)$, $C_s^*(1,\theta)-1$, from the uniform background values (for swimmer size $a = 1.00$ μm). We show the convergence of the solution as the number N of the Legendre modes in (3.34) are increased, i.e. $\boldsymbol{A} = \{A_0, \ldots, A_{N-1}, A_N\}$. (*b*) The deviations of the surface potential and ionic concentration as a function of swimmer size a (truncating at $N = 40$).

$$p - p_\infty = \gamma^{(1)} p^{(\gamma)} + \cdots \tag{3.43}$$

and the propulsion velocity about the stationary colloid, $\boldsymbol{U}^e = \boldsymbol{0}$

$$\boldsymbol{U}^e = \gamma^{(1)} \boldsymbol{U}^{e(\gamma)} + \cdots . \tag{3.44}$$

Then, the Stokes equations become

$$\nabla^2 \boldsymbol{v}^{(\gamma)} - \nabla p^{(\gamma)} = \boldsymbol{0}; \quad \nabla \cdot \boldsymbol{v}^{(\gamma)} = 0, \tag{3.45a,b}$$

with the slip boundary condition from matching to the inner solution,

$$\boldsymbol{v}^{(\gamma)}(1,\theta) = \boldsymbol{U}^{e(\gamma)} + \mu_e \frac{\partial \Phi^{(\gamma)}}{\partial \theta} \hat{\boldsymbol{e}}_\theta, \tag{3.46}$$

where $\mu_e = \zeta_0 + 4 \ln \cosh(\zeta_0/4)$. Recall that $\zeta_0 = \varphi_s$ is the ζ potential for the trivial solution with $\gamma^{(1)} = 0$.

Solving the homogeneous Stokes equations (3.45) with these boundary conditions gives the following structure for the flow generated by the electrophoretic and ionic-diffusiophoretic contributions:

$$\boldsymbol{v}(\boldsymbol{r}) = \gamma^{(1)} \boldsymbol{v}^{(\gamma)} = B_2[-\partial_z \boldsymbol{G}(\boldsymbol{r})] + B_1 \boldsymbol{D}(\boldsymbol{r}) + B_3[\partial_z^2 \boldsymbol{G}(\boldsymbol{r})] + O(r^{-4}), \tag{3.47}$$

expressed in terms of the leading-order fundamental singularities of the Stokes equation:

$$\boldsymbol{G}(\boldsymbol{r}) = \frac{\hat{\boldsymbol{e}}_z}{r} + \frac{\boldsymbol{r}\boldsymbol{r} \cdot \hat{\boldsymbol{e}}_z}{r^3}; \quad \boldsymbol{D}(\boldsymbol{r}) = 3\frac{\boldsymbol{r}\boldsymbol{r} \cdot \hat{\boldsymbol{e}}_z}{r^5} - \frac{\hat{\boldsymbol{e}}_z}{r^3}, \tag{3.48a,b}$$

with the strengths given by

$$B_1 = -\frac{1}{3}\mu_e \gamma^{(1)} A_1 \left(1 - \frac{3}{2}\frac{A_3}{A_1}\right); \quad B_2 = \frac{3}{2}\mu_e \gamma^{(1)} A_2; \quad B_3 = \frac{5}{4}\mu_e \gamma^{(1)} A_3, \tag{3.49a–c}$$

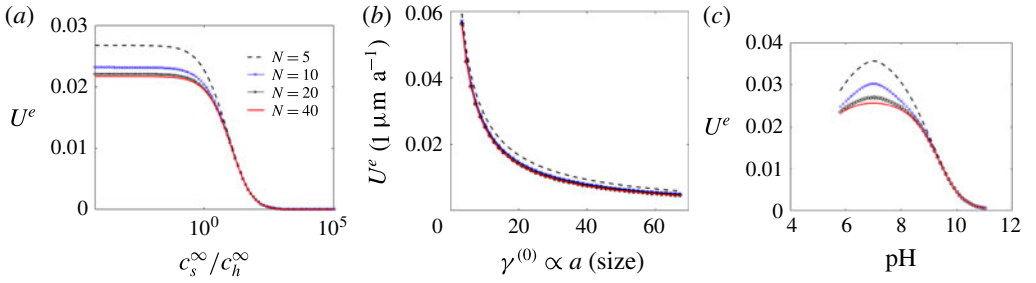

FIGURE 6. (Colour online) (Electrophoretic and ionic-diffusiophoretic contributions) (*a*) the propulsion speed U^e as a function of the salt concentration C_s^∞. (*b*) The propulsion speed U^e decays with increasing size a. (*c*) The speed U^e against the solution pH (we expect that the charge balance may be more complicated and the reaction kinetics are known to change with the solution pH (McKee 1969; Liu *et al.* 2014)).

where the A_l are obtained from solving equations (3.36). Imposing the constraint of zero total force, equation (3.6), leads to an expression for the electrophoretic and ionic-diffusiophoretic contributions to the propulsion velocity,

$$\boldsymbol{U}^e = -\tfrac{2}{3}\mu_e \gamma^{(1)} A_1 \hat{\boldsymbol{e}}_z. \tag{3.50}$$

Written in dimensional form (see figure 6),

$$\bar{\boldsymbol{U}}^e = -\frac{1}{3}\left(\frac{k_B T}{e}\right)^2 \frac{\epsilon}{\eta}\frac{A_1 \Delta k_{eff}^{(h)} c_{hp}^\infty}{D_h\left(c_h^\infty + c_s^\infty\right)}\left[\frac{e\bar{\zeta}_0}{k_B T} + 4\ln\cosh\left(\frac{e\bar{\zeta}_0}{4k_B T}\right)\right]\hat{\boldsymbol{e}}_z, \tag{3.51}$$

where $\bar{\zeta}_0 = (k_B T/e)\zeta_0$ is the average swimmer ζ potential. A plot of this electrophoretic contribution against the solution salt concentration (ionic strength) is shown in figure 6(*a*). As expected, this contribution is strongly sensitive to salt concentration. Interestingly, the swimmer speed is only weakly dependent on pH (see figure 6*c*) under weakly acidic conditions (high c_h^∞). This is due to the competition between the dependence on c_h^∞ of A_1 (decreases with c_h), μ_e (increases with c_h) and the denominator of the expression for $\boldsymbol{U}^e$ (increases with c_h). This is consistent with recent experiments (Brown & Poon 2014) which showed a minor reduction of swimming speed on addition of sodium hydroxide (NaOH). Furthermore, the propulsion speed is inversely dependent on swimmer size, a for large swimmer sizes as shown in figure 6(*b*). This is consistent with the experimental observation of $\sim 1/a$ propulsion velocity decay for large swimmer sizes (Howse *et al.* 2007).

3.2. *Self-diffusiophoresis*

In this section, we outline a solution of the equations of motion for the neutral solutes in the outer region ($\chi = L_{eff}/a \to 0$) to calculate the neutral-diffusiophoretic contribution to the propulsion velocity, $\boldsymbol{U}^d$. Detailed calculations for the inner interaction layer where the fields vary on the length scale L_{eff} can be found in the literature (Anderson *et al.* 1982; Golestanian *et al.* 2005, 2007; Howse *et al.* 2007; Michelin & Lauga 2014).

Here since there is a finite propulsion velocity, $\bar{\boldsymbol{U}}^d \neq 0$, for the uniformly coated system, $k_i^{(0)} \neq 0$, $k_i^{(1)} = 0$, then a weak variation of rates due to a varying thickness $k_i^{(0)} \gg k_i^{(1)}$ leads to a small correction which we can ignore. Hence we set $k_i^{(1)} = 0$ for the rest of this section.

3.2.1. *Dimensionless equations*

The position vector $\bar{\boldsymbol{r}}$ is measured in units of the swimmer size 'a', concentrations $\bar{c}_i$ in units of the steady-state background values c_i^{∞} (note that $\bar{c}_o$ is measured in units of c_{hp}^{∞}), the short-ranged interaction potential of solutes with the Janus sphere, $\bar{\Psi}$ in terms of the thermal energy scale $\beta^{-1} = k_B T$, neutral solute fluxes, $\bar{\boldsymbol{J}}_n$ in units of $D_n c_{hp}^{\infty}/a$, with D_i the diffusion coefficient of the ith solute. The fluid flow velocity $\bar{\boldsymbol{v}}$ is rescaled by $\bar{\mu}_d^{\ddagger} c_{hp}^{\infty}/a$, where $\bar{\mu}_d^{\ddagger}$ is the characteristic diffusiophoretic mobility, the pressure $\bar{p}$ is rescaled by $\bar{\mu}_d^{\ddagger}\eta c_{hp}^{\infty}/a^2$. Hence, the dimensionless quantities (no overbar) are expressed in terms of dimensional ones (with overbar) as follows $\boldsymbol{r} = (x, y, z) = \bar{\boldsymbol{r}}/a$, $c_i = \bar{c}_i/c_i^{\infty}$, $\Psi = \beta\bar{\Psi}$, $\boldsymbol{v} = \bar{\boldsymbol{v}}a/c_{hp}^{\infty}\bar{\mu}_d^{\ddagger}$, $p = \bar{p}a^2/c_{hp}^{\infty}\bar{\mu}_d^{\ddagger}\eta$. As before we define the dimensionless difference of the concentrations from their bulk values as $C_i(\boldsymbol{r}) \equiv c_i(\boldsymbol{r}) - 1 = (\bar{c}_i/c_i^{\infty}) - 1$.

The dimensionless equations for $r > 1$ in the outer region are thus Laplace equations for the concentration deviations

$$\nabla^2 C_o = 0, \tag{3.52}$$

$$\nabla^2 C_{hp} = 0, \tag{3.53}$$

and the Stokes equations for the fluid velocity, $\boldsymbol{v}(\boldsymbol{r})$

$$\boldsymbol{0} = \boldsymbol{\nabla}\cdot\boldsymbol{\Pi} = \nabla^2\boldsymbol{v} - \boldsymbol{\nabla}p; \quad 0 = \boldsymbol{\nabla}\cdot\boldsymbol{v}, \tag{3.54a,b}$$

where $p(\boldsymbol{r})$ is the hydrostatic pressure at $\boldsymbol{r}$ (Anderson 1989; Golestanian *et al.* 2005, 2007; Howse *et al.* 2007; Michelin & Lauga 2014).

3.2.2. *Dimensionless boundary conditions*

Matching with the inner layer (Anderson 1989; Golestanian *et al.* 2005, 2007; Howse *et al.* 2007; Michelin & Lauga 2014), gives rise to non-zero flux boundary conditions for hydrogen peroxide and oxygen

$$-\partial_r C_o|_{r=1} = \mathcal{J}_o(\theta)K(\cos\theta) = \frac{D_{hp}}{2D_o}\mathcal{K}_{eff}^{(hp)}(1 + C_{hp})K(\cos\theta), \tag{3.55}$$

$$-\partial_r C_{hp}\big|_{r=1} = \mathcal{J}_{hp}(\theta)K(\cos\theta) = -\mathcal{K}_{eff}^{(hp)}(1 + C_{hp})K(\cos\theta), \tag{3.56}$$

and vanishing concentration deviations far from the swimmer C_o, $C_{hp} \to 0$ as $r \to \infty$. $K(\cos\theta)$, the catalyst coverage function, is 1 on the platinum hemisphere and zero on the polystyrene hemisphere. From the reaction kinetics in appendix A, we obtain non-zero fluxes for hydrogen peroxide and oxygen

$$\mathcal{J}_o(\theta) = \frac{1}{2}\left(\frac{k_{eff}^{(hp)}\bar{c}_{hp}a}{D_o c_{hp}^{\infty}}\right)K(\cos\theta) = \frac{D_{hp}}{2D_o}\mathcal{K}_{eff}^{(hp)}(1 + C_{hp}(1,\theta))K(\cos\theta), \tag{3.57}$$

$$\mathcal{J}_{hp}(\theta) = -\left(\frac{k_{eff}^{(hp)}\bar{c}_{hp}a}{D_{hp}c_{hp}^{\infty}}\right)K(\cos\theta) = -\mathcal{K}_{eff}^{(hp)}(1 + C_{hp}(1,\theta))K(\cos\theta). \tag{3.58}$$

We have defined dimensionless $\mathcal{K}_{eff}^{(hp)} = k_{eff}^{(hp)}a/D_{hp}$, where $k_{eff}^{(hp)}\bar{c}_{hp} > 0$ is the effective rate of consumption of the hydrogen peroxide (see appendix A for details of the derivation).

The boundary conditions for the fluid velocity are

$$\boldsymbol{v}|_{r=1} = \boldsymbol{U}^d + \boldsymbol{v}^d_{slip}; \quad \boldsymbol{v}(r\to\infty) = \boldsymbol{0}, \tag{3.59a,b}$$

where $\boldsymbol{U}^d$ is the neutral self-diffusiophoretic contribution to the propulsion velocity. $\boldsymbol{v}^d_{slip} = \sum_{i\in\{o,hp\}} \mu_d^{(i)}(\mathbb{1} - \hat{\boldsymbol{n}}\hat{\boldsymbol{n}}) \cdot \boldsymbol{\nabla} C_i$ is the self-diffusiophoretic slip velocity obtained by matching with the inner solution (Anderson *et al.* 1982; Anderson 1989) and $\mathbb{1}$ is a unit matrix. The dimensionless self-diffusiophoretic mobility is given by $\mu_d^{(i)} = \lim_{\rho'\to\infty} \int_0^{\rho'} \rho[1 - e^{-\Psi_i(\rho)}]\,\mathrm{d}\rho$ (Anderson 1989).

Finally, the zero total force condition on the swimmer

$$\boldsymbol{F} = \oint_{r=1} \boldsymbol{\Pi} \cdot \hat{\boldsymbol{n}} \sin\theta\,\mathrm{d}\theta = \boldsymbol{0}, \tag{3.60}$$

determines the diffusiophoretic propulsion velocity $\boldsymbol{U}^d$.

3.2.3. *Outer concentration fields*

The general solution of the Laplace equations (3.52), (3.53) for the neutral solutes is of the form

$$C_o(r,\theta) = \sum_{l=0}^{\infty} \left(\frac{D_{hp}}{2D_o}\right) W_l \frac{P_l(\cos\theta)}{r^{l+1}}, \tag{3.61}$$

$$C_{hp}(r,\theta) = -\sum_{l=0}^{\infty} W_l \frac{P_l(\cos\theta)}{r^{l+1}}, \tag{3.62}$$

where $P_l(\cos\theta)$ are the Legendre polynomials and note that we have used the fact that $D_{hp}\mathcal{J}_{hp} + 2D_o\mathcal{J}_o = 0$. The amplitudes, W_l, are determined from either of the boundary conditions;

$$-\partial_r C_o|_{r=1} = \frac{D_{hp}}{2D_o}\mathcal{K}^{(hp)}_{eff}(1 + C_{hp})K(\cos\theta), \tag{3.63}$$

$$-\partial_r C_{hp}\big|_{r=1} = -\mathcal{K}^{(hp)}_{eff}(1 + C_{hp})K(\cos\theta). \tag{3.64}$$

This gives rise to a system of equations:

$$\sum_{l=0}^{\infty} W_l(l+1)P_l(\cos\theta) = \mathcal{K}^{(hp)}_{eff}\left(1 - \sum_{l=0}^{\infty} W_l P_l(\cos\theta)\right) K(\cos\theta). \tag{3.65}$$

From this, using the orthogonality condition of the Legendre polynomials, we obtain the linear system of equations for the amplitudes, W_l:

$$\boldsymbol{M}^{(d)} \cdot \boldsymbol{W} = \boldsymbol{\Lambda}^{(d)}, \tag{3.66}$$

where $\boldsymbol{W} = (W_0, \ldots, W_l, \ldots)$, and more explicitly

$$\begin{pmatrix} 1 & 0 & 0 & \cdots & 0 & \cdots \\ 0 & M^{(d)}_{11} & M^{(d)}_{12} & \cdots & M^{(d)}_{1l} & \cdots \\ 0 & M^{(d)}_{21} & M^{(d)}_{22} & \cdots & M^{(d)}_{2l} & \cdots \\ \vdots & \vdots & \vdots & \ddots & \vdots & \cdots \\ 0 & M^{(d)}_{n1} & M^{(d)}_{n2} & \cdots & M^{(d)}_{nl} & \cdots \\ \vdots & \vdots & \vdots & \vdots & \vdots & \ddots \end{pmatrix} \begin{pmatrix} W_0 \\ W_1 \\ W_2 \\ \vdots \\ W_l \\ \vdots \end{pmatrix} = \begin{pmatrix} 0 \\ \Lambda^{(d)}_1 \\ \Lambda^{(d)}_2 \\ \vdots \\ \Lambda^{(d)}_n \\ \vdots \end{pmatrix}, \tag{3.67}$$

where the matrix $\boldsymbol{M}^{(d)}$ and vector $\boldsymbol{\Lambda}^{(d)}$ entries are given by

$$M_{nl}^{(d)} = \delta_{nl} + \mathcal{K}_{eff}^{(hp)} \left(\frac{n+\frac{1}{2}}{n+1} \right) \int_0^1 P_n(x) P_l(x)\, \mathrm{d}x, \tag{3.68}$$

$$\Lambda_n^{(d)} = \mathcal{K}_{eff}^{(hp)} \left(\frac{n+\frac{1}{2}}{n+1} \right) \int_0^1 P_n(x)\, \mathrm{d}x. \tag{3.69}$$

Here as in the ionic section, we solve a truncated approximation of the linear equations above, including all modes up to the Nth Legendre mode$\{W_0, W_1, \ldots, W_N\}$. As above, we can obtain analytic asymptotic solutions for $\mathcal{K}_{eff}^{(hp)} \ll 1$ and $\mathcal{K}_{eff}^{(hp)} \gg 1$:
$\mathcal{K}_{eff}^{(hp)} \ll 1$: In this regime, $W_l \sim \Lambda_l^{(d)}$ and

$$W_1 \sim \tfrac{3}{8} \mathcal{K}_{eff}^{(hp)} \tag{3.70}$$

$\mathcal{K}_{eff}^{(hp)} \gg 1$: In this regime,

$$W_1 \sim \Xi, \tag{3.71}$$

where $\Xi > 0$ is some constant to be determined numerically. Since $\mathcal{K}_{eff}^{(hp)} \propto a$ (swimmer size), this implies the limit $\mathcal{K}_{eff}^{(hp)} \gg 1$ corresponds to large swimmer size. For $a = 1.00\ \mu\mathrm{m}$ sized swimmer in 10 % w/v H_2O_2 solution, and the measured reaction rates in table 1, the estimate of the dimensionless reaction rate coefficient is $\mathcal{K}_{eff}^{(hp)} \approx 0.026$. Hence, this puts the current experimental measurements (Brown & Poon 2014; Ebbens *et al.* 2014) in the first regime ($W_l \sim \Lambda_l^{(d)}$). We note that in this regime $C_{hp} \sim W_l \sim \mathcal{K}_{eff}^{(hp)} \ll 1$.

The coefficients W_l determine the solute concentration, and hence the slip velocity which act as boundary conditions for the Stokes flow problem. Hence the velocity fields generated, expressed in terms of the fundamental singularities (see (3.48)) of the Stokes flow are

$$\boldsymbol{v}(\boldsymbol{r}) = B_1^{(d)} \boldsymbol{D}(\boldsymbol{r}) + B_3^{(d)} [\partial_z^2 \boldsymbol{G}(\boldsymbol{r})] + O(r^{-4}), \tag{3.72}$$

where the coefficients $(B_1^{(d)}, B_3^{(d)})$ are

$$B_1^{(d)} = -\frac{1}{3} \mu_d W_1 \left(1 - \frac{3}{2} \frac{W_3}{W_1} \right); \quad B_3^{(d)} = \frac{5}{4} \mu_d W_3. \tag{3.73a,b}$$

Imposing the condition of net zero total force, we obtain the neutral-diffusiophoretic contribution to the propulsion velocity as

$$\boldsymbol{U}^d = -\sum_{i \in \{hp, o\}} \frac{1}{4\pi} \int_0^{2\pi} \mathrm{d}\phi \int_0^{\pi} \sin\theta\, \mathrm{d}\theta\, \mu_d^{(i)} \left(\mathbb{1} - \hat{\boldsymbol{n}}\hat{\boldsymbol{n}} \right) \cdot \boldsymbol{\nabla} C_i, \tag{3.74}$$

where since we have taken the interaction potential, Ψ identical for all species, we have identical neutral-diffusiophoretic mobilities for all the neutral solute species, $\mu_d^{(i)} = 1, i \in \{o, hp\}$. From the modes calculated above, we thus obtain

$$\boldsymbol{U}^d = -\tfrac{2}{3} \mu_d W_1 \hat{\boldsymbol{e}}_z, \tag{3.75}$$

where $\mu_d = \mu_d^{(hp)} - (D_{hp}/2D_o)\mu_d^{(o)} = 1 - (D_{hp}/2D_o)$ is the combined effective diffusiophoretic mobility.

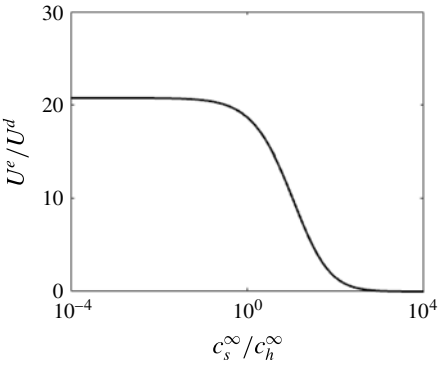

FIGURE 7. Plot of comparison of the ionic solute contribution to the neutral solute contribution (3.77) for system parameters in table 1 and pH = 5.8.

3.3. *Comparison of ionic and neutral velocities*

Finally, we can now compare the two contributions to the swimmer propulsion from ionic and neutral solutes using dimensional quantities. From (3.50) and (3.75), the relative speed

$$\frac{\bar{U}^e}{\bar{U}^d} = \frac{\left(\epsilon k_B^2 T^2/a\eta e^2\right) U^e}{\left(\bar{\mu}_d^{\ddagger} c_{hp}^\infty/a\right) U^d} = \frac{\bar{\mu}_e}{\bar{\mu}_d} \frac{(k_B T/e)\gamma^{(1)} A_1}{c_{hp}^\infty W_1}, \tag{3.76}$$

where $\bar{\mu}_e = (\epsilon k_B T/e\eta)\,\mu_e$ is the electrophoretic mobility and $\bar{\mu}_d = \mu_d \bar{\mu}_d^{\ddagger}$ is the diffusiophoretic mobility, both in dimensional form. For a fixed swimmer size, and in the limit $\gamma^{(0)} \ll 1, \mathcal{K}_{eff}^{(hp)} \ll 1$, the above ratio takes the simple analytic expression

$$\frac{\bar{U}^e}{\bar{U}^d} = \frac{1}{6} \frac{\bar{\mu}_e}{\bar{\mu}_d} \frac{D_{hp}}{D_h} \frac{\Delta k_{eff}^{(h)}}{k_{eff}^{(hp)}} \frac{(k_B T/e)}{(c_s^\infty + c_h^\infty)}, \tag{3.77}$$

where $k_{eff}^{(hp)} c_{hp}^\infty > 0$ is the effective rate of the hydrogen peroxide consumption and $\Delta k_{eff}^{(h)} > 0$ is the scale of the difference between the rates at the pole and equator due to the Pt thickness variation (defined in appendix A for a particular example of reaction model). These rates are linear functions of the c_{hp}^∞ concentration for low fuel concentration. In figure 7, it can be seen that the electrophoretic contribution vanishes at large ionic strengths and the swimmer speed asymptotically approaches the diffusiophoretic contribution value $\bar{U}^d$. The self-diffusiophoretic speed $\bar{U}^d = \bar{\mu}_d k_{eff}^{(hp)} c_{hp}^\infty / 4D_{hp} \sim 0.52\ \mu\mathrm{ms}^{-1}$ (see table 1) for the chosen system parameter values in the plot (figure 7).

4. Summary and discussion

The total propulsion velocity of the metallic-insulator sphere from both electrophoresis and diffusiophoresis, from (3.50) and (3.75), in dimensional form is

$$\bar{\boldsymbol{U}} = -\left[\frac{1}{3}\bar{\mu}_e \frac{\Delta k_{eff}^{(h)} c_{hp}^\infty}{D_h \left(c_s^\infty + c_h^\infty\right)} \left(\frac{k_B T}{e}\right) A_1 + \frac{2}{3}\bar{\mu}_d \frac{c_{hp}^\infty}{a} W_1\right] \hat{\boldsymbol{e}}_z, \tag{4.1}$$

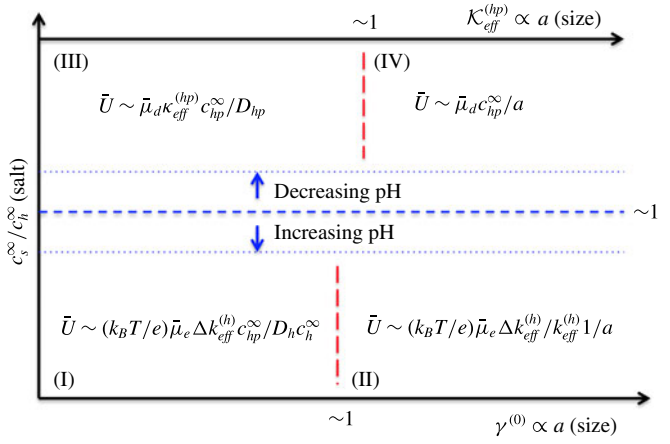

FIGURE 8. (Colour online) Asymptotic regimes of the swimmer propulsion speed $\bar{U}$. The dimensionless parameters on the horizontal axes are $\gamma^{(0)} = k_{eff}^{(h)} c_{hp}^{\infty} a/D_h \sum_{i\in ions} c_i^{\infty}$ and $\mathcal{K}_{eff}^{(hp)} = k_{eff}^{(hp)} a/D_{hp}$ where D_i and c_i^{∞} are respectively the diffusion coefficient and bulk concentration of chemical species i. $k_{eff}^{(i)}$ is the average rate of production/consumption of species i on the catalytic coated hemisphere. $\Delta k_{eff}^{(i)}$ is the difference in the reaction rate between the equator where the coating is thinnest and the pole where the coating is thickest. $\bar{\mu}_e$ and $\bar{\mu}_d$ are electrophoretic and diffusiophoretic mobilities respectively.

where $\bar{\mu}_e$ and $\bar{\mu}_d$ are the electrophoretic and diffusiophoretic mobilities. The scale of the difference between the rates at the poles and equator due to the Pt thickness variation $\Delta k_{eff}^{(h)} > 0$ is defined in appendix A for a particular reaction kinetic model. We point out that these results are qualitatively independent of the details of the reaction kinetics, provided the reaction involves both charged and neutral pathways for the reduction of the hydrogen peroxide and the reaction rate varies along the catalytic cap.

The ionic contribution to the expression above has a number of important simple features that are in agreement with recent experimental results on this system (Howse *et al.* 2007; Ebbens *et al.* 2012; Brown & Poon 2014; Ebbens *et al.* 2014; Das *et al.* 2015): (i) it depends linearly on the fuel, c_{hp}^{∞}, at low concentrations and the dependence weakens at high concentrations, (ii) it is independent of a at small a and behaves as $1/a$ for large a due to fuel depletion as shown in Ebbens *et al.* (2012) and (iii) it is a monotonically decreasing function of salt concentration, c_s^{∞} starting from a finite value when $c_s^{\infty} = 0$ and tending to zero as c_s^{∞} becomes large. Hence at high salt concentration the swimming speed saturates to the neutral-diffusiophoretic value (see figure 7). The electrophoretic contribution, which can be much larger than the diffusiophoretic part, vanishes if there is no variation in the rates k_i on the surface.

Adding salt to the solution containing the swimmer would influence the propulsion in three possible ways (i) pH neutral salts that do not specifically adsorb to the surface would enhance the solution conductivity thereby reducing the effective screening length (ii) while alkali or acidic salts would in general alter the total surface charge in addition to the increased solution conductivity, (iii) Pt catalytic decomposition of H_2O_2 is known to strongly depend on the solution pH (McKee 1969; Liu *et al.* 2014). Hence, non-pH neutral salts would also affect the Pt catalytic activity.

We note also that due to the existence of the two separate reaction loops, the overall catalytic reaction rate (measured from the current J_o above) can be significantly reduced with only small reductions to the swimming speed; say by a significant decrease in k_1. This type of behaviour would be expected from any reaction scheme which has this topological structure.

In conclusion, we have shown that in a system with catalytic reaction with charged intermediates, the existence of thickness dependence in the reaction rates up to a certain limit (a few nanometres), allows us to create – by tapering the catalyst layer – spatially separated non-equilibrium cycles that could lead to large-scale (many microns) ionic currents in the form of closed loops in the bulk. This remarkable effect, combining long-range electrostatic interactions with non-equilibrium chemical reactions to substantially enhance surface generated flows has potential for application in many different areas of nanoscience.

Acknowledgements

This work was supported by EPSRC grant EP/G026440/1 (T.B.L., Y.I.), and HFSP grant RGP0061/2013 (R.G.). Y.I. acknowledges the support of University of Bristol. T.B.L. acknowledges support of BrisSynBio, a BBSRC/EPSRC Advanced Synthetic Biology Research Centre (grant no. BB/L01386X/1).

Appendix A. Reaction kinetics

In this section, our goal is to obtain the fluxes on the surface of the swimmer, $\bar{\mathcal{J}}_i$ of all the chemical species involved in the H_2O_2 decomposition

$$\mathrm{Pt} + 2\mathrm{H_2O_2} \rightarrow \boxed{\text{Intermediate complexes}} \rightarrow \mathrm{Pt} + 2\mathrm{H_2O} + \mathrm{O_2}. \tag{A 1}$$

Though a complete picture of the intermediate complexes in reaction (A 1) remains elusive, it is known that there are neutral pathways as well as ionic electrochemical pathways (Hall, Khudaish & Hart 2000; Katsounaros *et al.* 2012). However, we find that our results are qualitatively independent of many details of the reaction scheme considered as long as they involve both neutral and charged pathways. So our lack of knowledge of the microscopic chemical kinetics is not such a hindrance. To illustrate this, we consider two different reaction schemes involving a neutral as well as a charged pathway. We emphasize that both schemes are provided simply as examples as the precise details of the chemical kinetics are not known.

A.1. *Reaction scheme 1*

First, we consider a reaction scheme for the reaction (A 1) made up of two pathways, one neutral

$$\mathrm{Pt} + 2\mathrm{H_2O_2} \xrightarrow{k_0} \mathrm{Pt\,(H_2O_2)} + \mathrm{H_2O_2} \xrightarrow{k_1} \mathrm{Pt\,(H_2O_2)_2} \xrightarrow{k_2} \mathrm{Pt} + 2\mathrm{H_2O} + \mathrm{O_2}, \tag{A 2}$$

and the other ionic involving charged intermediates,

$$\mathrm{Pt} + 2\mathrm{H_2O} \underset{k_{-3}}{\overset{k_3}{\rightleftharpoons}} \mathrm{Pt\,(H_2O_2)} + 2e^- + 2\mathrm{H^+}. \tag{A 3}$$

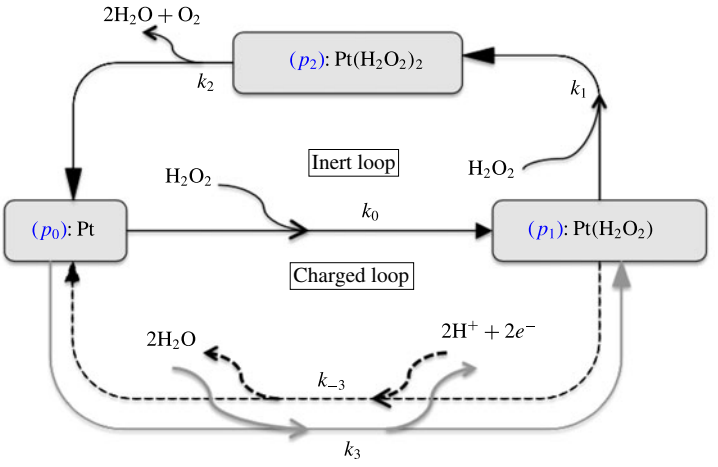

FIGURE 9. (Colour online) (Reaction scheme 1): schematic complexation kinetics of the platinum catalyst with free (0th state) Pt occupied with probability density p_0; first complex state $Pt(H_2O_2)$ occupied with probability density p_1 and the second complex state $Pt(H_2O_2)_2$ occupied with probability density p_2.

The reaction scheme above and the intermediate states denoted by (0, 1, 2) are enumerated in figure 9. The kinetics of the Pt catalyst complexation in stationary state reads

$$0 = \partial_t p_0 = -k_0 \bar{c}_{hp} p_0 - k_3 p_0 + k_2 p_2 + k_{-3} \bar{c}_h^2 p_1, \tag{A 4}$$

$$0 = \partial_t p_1 = k_0 \bar{c}_{hp} p_0 + k_3 p_0 - k_1 \bar{c}_{hp} p_1 - k_{-3} \bar{c}_h^2 p_1, \tag{A 5}$$

$$0 = \partial_t p_2 = k_1 \bar{c}_{hp} p_1 - k_2 p_2, \tag{A 6}$$

where p_i are the complexation probabilities. Solving for these probabilities p_i, we obtain

$$p_0 = \mathcal{M}^{-1} k_2 \left(k_1 \bar{c}_{hp} + k_{-3} \bar{c}_h^2 \right), \tag{A 7}$$

$$p_1 = \mathcal{M}^{-1} k_2 \left(k_0 \bar{c}_{hp} + k_3 \right), \tag{A 8}$$

$$p_2 = \mathcal{M}^{-1} k_1 \bar{c}_{hp} \left(k_0 \bar{c}_{hp} + k_3 \right), \tag{A 9}$$

where the normalization condition $p_0 + p_1 + p_2 = 1$ was used and we have defined

$$\mathcal{M} := k_2 k_3 + k_2 k_{-3} \bar{c}_h^2 + (k_0 k_2 + k_1 k_3 + k_1 k_2)\, \bar{c}_{hp} + k_0 k_1 \bar{c}_{hp}^2. \tag{A 10}$$

This leads to expressions for the fluxes $\bar{\mathcal{J}}_i$ of $i \in \{o, hp, h\}$

$$\begin{aligned} \bar{\mathcal{J}}_o(\theta) &= k_2 p_2 K(\cos\theta), \\ &= \mathcal{M}^{-1} k_1 k_2 \bar{c}_{hp} (k_0 \bar{c}_{hp} + k_3) K(\cos\theta), \end{aligned} \tag{A 11}$$

$$\begin{aligned} \bar{\mathcal{J}}_{hp}(\theta) &= -(k_0 p_0 + k_1 p_1)\, \bar{c}_{hp} K(\cos\theta), \\ &= -\mathcal{M}^{-1} k_2 \bar{c}_{hp} (k_1 k_3 + k_0 k_{-3} \bar{c}_h^2 + 2 k_0 k_1 \bar{c}_{hp}) K(\cos\theta), \end{aligned} \tag{A 12}$$

$$\begin{aligned} \bar{\mathcal{J}}_h(\theta) &= 2 \left(k_3 p_0 - k_{-3} \bar{c}_h^2 p_1 \right) K(\cos\theta), \\ &= 4 \mathcal{M}^{-1} k_2 \bar{c}_{hp} (k_1 k_3 - k_0 k_{-3} \bar{c}_h^2) K(\cos\theta), \end{aligned} \tag{A 13}$$

and for the fluxes of hydroxide and the salt, $\bar{\mathcal{J}}_{oh}=0$, $\bar{\mathcal{J}}_{s,\pm}=0$. Measurements of the reaction rates (Ebbens *et al.* 2014) imply that $\bar{\mathcal{J}}_{hp}$ and $\bar{\mathcal{J}}_{o}$ vary with the Pt coating thickness (of $\sim$nm scale). Hence we may assume that the rate 'constants' k_i vary in a similar manner.

Since the thickness of the coating varies across the Pt cap, the reaction rates $k_i(\theta)$ vary over the coated hemisphere, and can be expanded in Legendre polynomials. We consider a simple linear approximation

$$k_i(\theta) \cong k_i^{(0)} + k_i^{(1)} \cos\theta, \tag{A 14}$$

in $\cos\theta$ and we assume a weak variation $k_i^{(1)}/k_i^{(0)} \ll 1$ of the rates.

The solute fluxes $\bar{\mathcal{J}}_i$ above in (A 11)–(A 13) require the inner (Debye-layer) proton concentration profile

$$\bar{c}_h(1,\theta)/c_h^{\infty} = (1+C_h(1,\theta))\, e^{-\zeta(\theta)}; \quad \zeta(\theta)=\varphi_s-\Phi(1,\theta), \tag{A 15a,b}$$

from (B 22) in appendix B, where $C_h(1,\theta)$ and $\Phi(1,\theta)$ are the deviations from the uniform background of proton concentration and electric fields. φ_s is the electric potential on the swimmer surface. We have taken φ_s constant here, but it is straightforward to generalize our calculations to situations in which it varies across the surface. We note that having an electric potential difference between the coated and non-coated hemispheres does not lead to qualitative differences from the results presented here. Hence, the proton flux at the outer edge of the double layer reads

$$\bar{\mathcal{J}}_h(\theta) = 4\mathcal{M}^{-1}k_2\bar{c}_{hp}(k_1k_3 - k_0k_{-3}(c_h^{\infty})^2(1+C_h)^2e^{-2\zeta(\theta)})K(\cos\theta). \tag{A 16}$$

Furthermore, Taylor expanding the flux up to linear order in $k_i^{(1)}$, and the deviations C_h, Φ;

$$\bar{\mathcal{J}}_h(\theta) = \left(\bar{\mathcal{J}}_h^{(0)} + \bar{\mathcal{J}}_h^{(1)}P_1(\cos\theta) + \bar{\mathcal{J}}_h^{\prime(0)}\,(\Phi+C_h)\right) K(\cos\theta), \tag{A 17}$$

where $j=\{0,1,2\}$. We define

$$\bar{\mathcal{J}}_h^{(0)} = 4\{k_2c_{hp}\}^{(0)}\left(\{k_1k_3\}^{(0)} - \{k_0k_{-3}\}^{(0)}(c_h^{\infty})^2e^{-2\varphi_s}\right)/\mathcal{M}^{(0)}, \tag{A 18}$$

$$\bar{\mathcal{J}}_h^{(1)} = 4\{k_2c_{hp}\}^{(0)}\left(\{k_1k_3\}^{(1)} - \{k_0k_{-3}\}^{(1)}(c_h^{\infty})^2e^{-2\varphi_s}\right)/\mathcal{M}^{(0)}, \tag{A 19}$$

$$\bar{\mathcal{J}}_h^{\prime(0)} = 8\{k_2c_{hp}\}^{(0)}\{k_0k_{-3}\}^{(0)}(c_h^{\infty})^2e^{-2\varphi_s}/\mathcal{M}^{(0)}, \tag{A 20}$$

$$\mathcal{M}^{(0)} = \left\{k_2k_3 + k_2k_{-3}\bar{c}_h^2 + (k_0k_2+k_1k_3+k_1k_2)\,\bar{c}_{hp} + k_0k_1\bar{c}_{hp}^2\right\}^{(0)}. \tag{A 21}$$

Now, imposing net charge conservation, equation (2.16), on the swimmer surface, equation (A 17) for the proton flux leads to

$$\bar{\mathcal{J}}_h^{(0)} + \frac{1}{2}\bar{\mathcal{J}}_h^{(1)} + \bar{\mathcal{J}}_h^{\prime(0)}\int_0^{\pi}(\Phi+C_h)\,K(\cos\theta)\sin\theta\,\mathrm{d}\theta = 0. \tag{A 22}$$

Then, substituting for $\bar{\mathcal{J}}_h^{(i)}$ (from (A 18)–(A 20)) and simplifying;

$$(c_h^{\infty})^2e^{-2\varphi_s}\left(1+\frac{1}{2}\frac{\{k_0k_{-3}\}^{(1)}}{\{k_0k_{-3}\}^{(0)}} + 2\int_0^{\pi}(\Phi+C_h)\,K(\cos\theta)\sin\theta\,\mathrm{d}\theta\right) \tag{A 23}$$

$$= \frac{\{k_1k_3\}^{(0)}}{\{k_0k_{-3}\}^{(0)}} + \frac{1}{2}\frac{\{k_1k_3\}^{(1)}}{\{k_0k_{-3}\}^{(0)}}. \tag{A 24}$$

For a uniform coating (i.e. $k_i^{(1)} = 0$ for all i), which has the trivial solution $\Phi = C_h = 0$, the zero total current condition gives rise to

$$(c_h^\infty)^2 e^{-2\varphi_s} \cong \frac{\{k_1 k_3\}^{(0)}}{\{k_0 k_{-3}\}^{(0)}}, \tag{A 25}$$

which is all that is required for a linear expansion about a uniform coating. Hence solving for the swimmer potential φ_s, we obtain the equation

$$\varphi_s = \varphi_s^\ominus - \ln 10 \mathrm{pH}, \tag{A 26}$$

where $\mathrm{pH} = -\log_{10} c_h^\infty$ (with c_h^∞ measured in molar units) and

$$\varphi_s^\ominus = -\frac{1}{2} \ln \left(\frac{\{k_1 k_3\}^{(0)}}{\{k_0 k_{-3}\}^{(0)}} \right). \tag{A 27}$$

Therefore, eliminating the swimmer potential and proton background concentration (φ_s, c_h^∞) by substituting (A 25) into (A 17) and keeping only linear perturbations, the proton flux assumes a simple form

$$\boxed{\bar{\mathcal{J}}_h(\theta) \cong \left[\Delta k_{eff}^{(h)} (1 - 2\cos\theta) - k_{eff}^{(h)} \delta(\Phi + C_h) \right] c_{hp}^\infty K(\cos\theta),} \tag{A 28}$$

where we have defined

$$k_{eff}^{(h)} = \frac{8\{k_1 k_2 k_3\}^{(0)}}{\mathcal{M}^{(0)}}; \tag{A 29}$$

$$\Delta k_{eff}^{(h)} = \frac{k_{eff}^{(h)}}{2} \left(\frac{\{k_0 k_{-3}\}^{(1)}}{\{k_0 k_{-3}\}^{(0)}} - \frac{\{k_1 k_3\}^{(1)}}{\{k_1 k_3\}^{(0)}} \right), \tag{A 30}$$

$$\delta(\Phi + C_h) = \left[(\Phi + C_h) - \int_0^\pi (\Phi + C_h) K(\cos\theta) \sin\theta \, \mathrm{d}\theta \right]. \tag{A 31}$$

$k_{eff}^{(h)} c_{hp}^\infty > 0$ is the typical scale of the average proton consumption and production and $\Delta k_{eff}^{(h)} c_{hp}^\infty$ the scale of the difference between the rates at the pole and equator due to variation of coating thickness over the surface. $\delta(\Phi + C_h)$ is the deviation of the perturbative fields from their surface average; which promotes/penalize the oxidation/reduction reactions. The proton flux $\bar{\mathcal{J}}_h$ is linear in c_{hp}^∞ for low fuel concentration and the dependence weakens for high fuel concentration. It is noteworthy that with uniform coating, $k_i = k_i^{(0)} \Rightarrow \Delta k_{eff}^{(h)} = 0$ and the deviation fields vanish ($\Phi = 0 = C_i$).

The fluxes of neutral solutes from (A 11), (A 12) give

$$\bar{\mathcal{J}}_o(\theta) \cong \tfrac{1}{2} k_{eff}^{(hp)} \bar{c}_{hp}(1, \theta), \tag{A 32}$$

$$\bar{\mathcal{J}}_{hp}(\theta) \cong -k_{eff}^{(hp)} \bar{c}_{hp}(1, \theta), \tag{A 33}$$

where the effective rate of hydrogen peroxide consumption is defined

$$k_{eff}^{(hp)} = \frac{2}{\mathcal{M}^{(0)}} \{k_0 k_1 k_2\}^{(0)} \bar{c}_{hp}(1, \theta) + \frac{1}{2} k_{eff}^{(h)}, \tag{A 34}$$

and the effective rate of proton consumption/desorption $k_{eff}^{(h)}$ is defined in (A 29). Note that $\bar{\mathcal{J}}_{hp}$ and $\bar{\mathcal{J}}_o$ are linear in c_{hp}^∞ for low fuel (c_{hp}^∞) concentration, and show the saturation typical of Michaelis–Menten kinetics at high fuel concentration.

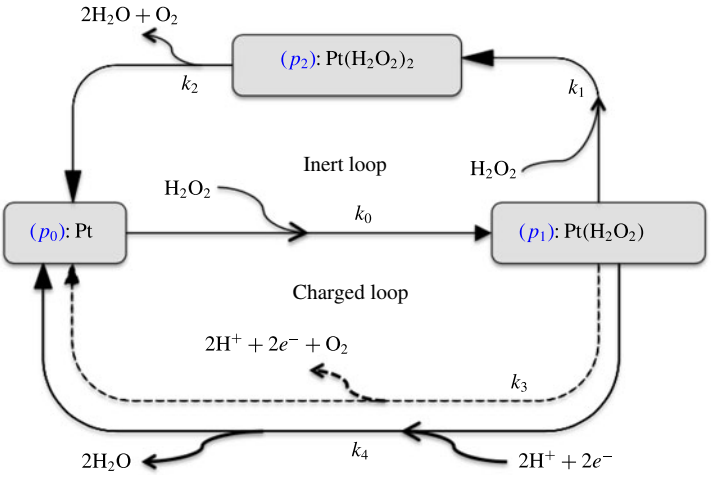

FIGURE 10. (Colour online) (Reaction scheme 2): schematic complexation kinetics of the platinum catalyst with free (0th state) Pt occupied with probability density p_0; first complex state $Pt(H_2O_2)$ occupied with probability density p_1, and the second complex state $Pt(H_2O_2)_2$ occupied with probability density p_2.

A.2. *Reaction scheme 2*

Alternatively, we may consider a different reaction scheme, with the same neutral pathway

$$Pt + 2H_2O_2 \xrightarrow{k_0} Pt\,(H_2O_2) + H_2O_2 \xrightarrow{k_1} Pt\,(H_2O_2)_2 \xrightarrow{k_2} Pt + 2H_2O + O_2, \tag{A 35}$$

but with a different electrochemical pathway

$$Pt\,(H_2O_2) \xrightarrow{k_3} Pt + 2H^+ + 2e^- + O_2, \tag{A 36}$$

$$Pt\,(H_2O_2) + 2H^+ + 2e^- \xrightarrow{k_4} Pt + 2H_2O. \tag{A 37}$$

This is the reaction scheme commonly used in modelling the electrophoretic motion of the bimetallic nanorods (Kline *et al.* 2005*a*,*b*; Paxton *et al.* 2005; Dhar *et al.* 2006; Sabass & Seifert 2012). As for the reaction scheme considered in the previous section, we can write down the equations of motion for the kinetics for this scheme (see figure 10). Hence, we can, as in the previous section, obtain the fluxes $\bar{\mathcal{J}}_i$,

$$\bar{\mathcal{J}}_h(\theta) = 2\,\mathcal{M}^{-1}\,k_0k_2\bar{c}_{hp}\left(k_3 - k_4\bar{c}_h^2\right)\,K(\cos\theta), \tag{A 38}$$

$$\bar{\mathcal{J}}_{hp}(\theta) = -\mathcal{M}^{-1}\,k_0k_2\bar{c}_{hp}\left(2k_1\bar{c}_{hp} + k_3 + k_4\bar{c}_h^2\right)\,K(\cos\theta), \tag{A 39}$$

$$\bar{\mathcal{J}}_o(\theta) = \mathcal{M}^{-1}\,k_0k_2\bar{c}_{hp}\left(k_1\bar{c}_{hp} + k_3\right)\,K(\cos\theta), \tag{A 40}$$

where here $\mathcal{M} := k_2k_3 + (k_0 + k_1)\,k_2\bar{c}_{hp} + k_2k_4\bar{c}_h^2 + k_0k_1\bar{c}_{hp}^2$.

Now, imposing the steady-state constraint $\oint \bar{\mathcal{J}}_h(\theta)\,\mathrm{d}\cos\theta = 0$, and following the same procedure as in the previous section (with $k_i = k_i^{(0)} + k_i^{(1)}\cos\theta$), we obtain the same expression for the proton flux as (A 28)

$$\bar{\mathcal{J}}_h(\theta) \cong [\Delta k_{eff}^{(h)}(1 - 2\cos\theta) - k_{eff}^{(h)}\delta(\Phi + C_h)]\bar{c}_{hp}^{\infty}K(\cos\theta), \tag{A 41}$$

where here we have

$$k_{eff}^{(h)} = \frac{4\{k_0 k_2 k_3\}^{(0)}}{\mathcal{M}^{(0)}}; \quad \Delta k_{eff}^{(h)} = \frac{k_{eff}^{(h)}}{2}\left(\frac{k_4^{(1)}}{k_4^{(0)}} - \frac{k_3^{(1)}}{k_3^{(0)}}\right). \tag{A 42a,b}$$

The deviation $\delta(\Phi + C_h) = [(\Phi + C_h) - \int_0^{\pi}(\Phi + C_h)K(\cos\theta)\sin\theta\,\mathrm{d}\theta]$ retains its previous definition as given in (A 31). Finally, we obtain the same relation $\varphi_s = \varphi_s^{\ominus} - \ln 10\mathrm{pH}$ and the kinetically defined potential for this scheme is $\varphi_s^{\ominus} = -(1/2)\ln(k_3^{(0)}/k_4^{(0)})$.

It is noteworthy that both reaction schemes possess many similar qualitative features: the solute fluxes $\bar{\mathcal{J}}_i$ retain the same functional dependence on the fuel concentration $\bar{c}_{hp}$ and the variation in reaction rates.

Appendix B. Derivation of the slip velocity

In the Debye layer, where the fields vary on the Debye length scale κ^{-1}, we rescale the radial coordinate by the $\lambda = (\kappa a)^{-1}$,

$$\rho = \frac{r-1}{\lambda}, \tag{B 1}$$

and expand the deviation fields in the form

$$C_i(r,\theta) = \mathcal{C}_i^{(0)}(\rho,\theta) + \lambda\mathcal{C}_i^{(1)}(\rho,\theta) + \cdots, \tag{B 2}$$
$$\Phi(r,\theta) = \varphi^{(0)}(\rho,\theta) + \lambda\varphi^{(1)}(\rho,\theta) + \cdots \tag{B 3}$$
$$\boldsymbol{v}(r,\theta) = \boldsymbol{\mathcal{V}}^{(0)}(\rho,\theta) + \lambda\boldsymbol{\mathcal{V}}^{(1)}(\rho,\theta) + \cdots, \tag{B 4}$$
$$p(r,\theta) = \lambda^{-2}\mathcal{P}^{(-2)}(\rho,\theta) + \lambda^{-1}\mathcal{P}^{(-1)}(\rho,\theta) + \cdots, \tag{B 5}$$

where $i \in \{h, oh, s\pm\}$. It is noteworthy that the expansion for the pressure field begins with $\mathcal{P}^{(-2)}$ to balance $O(\lambda^{-2})$ radial electric stresses that could not be accounted by the viscous stresses at the interface (Anderson 1989; Yariv 2011).

B.1. *Ionic solute concentrations*

Exploiting the axisymmetry of the problem, we write the steady-state Nernst–Planck equations (3.1) in spherical polar coordinates, with only radial and polar angle dependence:

$$\boldsymbol{\nabla}\cdot\boldsymbol{J}_i(r,\theta) = \left(\frac{\partial}{\partial r} + \frac{2}{r}\right)J_{i,r} + \frac{1}{r}\left(\frac{\partial}{\partial\theta} + \cot\theta\right)J_{i,\theta} = 0, \tag{B 6}$$

where

$$J_{i,\theta} = -r^{-1}\partial_\theta C_i - z_i(1+C_i)r^{-1}\partial_\theta\Phi \tag{B 7}$$
$$J_{i,r} = -\partial_r C_i - z_i(1+C_i)\partial_r\Phi. \tag{B 8}$$

We therefore expand the fluxes in the inner coordinates (ρ,θ), noting that $r = \lambda\rho + 1$

$$\boldsymbol{J}_i(r,\theta) = \boldsymbol{\mathfrak{J}}_i(\rho,\theta) = \lambda^{-1}\boldsymbol{\mathfrak{J}}_i^{(-1)}(\rho,\theta) + \boldsymbol{\mathfrak{J}}_i^{(0)}(\rho,\theta) + O(\lambda), \tag{B 9}$$

where we define radial and polar components of the currents (see (B 2) and (B 3))

$$\mathfrak{J}^{(-1)}_{i,\theta}(\rho,\theta)=0, \tag{B 10}$$

$$\mathfrak{J}^{(-1)}_{i,\rho}(\rho,\theta)=-\frac{\partial \mathcal{C}^{(0)}_i}{\partial\rho}-z_i\left(1+\mathcal{C}^{(0)}_i\right)\frac{\partial\varphi^{(0)}}{\partial\rho}, \tag{B 11}$$

$$\mathfrak{J}^{(0)}_{i,\theta}(\rho,\theta)=-\frac{\partial \mathcal{C}^{(0)}_i}{\partial\theta}-z_i\left(1+\mathcal{C}^{(0)}_i\right)\frac{\partial\varphi^{(0)}}{\partial\theta}, \tag{B 12}$$

$$\mathfrak{J}^{(0)}_{i,\rho}(\rho,\theta)=-\frac{\partial \mathcal{C}^{(1)}_i}{\partial\rho}-z_i\frac{\partial\varphi^{(1)}}{\partial\rho}-z_i\mathcal{C}^{(1)}_i\frac{\partial\varphi^{(0)}}{\partial\rho}. \tag{B 13}$$

Hence, equation (B 6) can be written

$$\boldsymbol{\nabla}\cdot\boldsymbol{\mathfrak{J}}_i(\rho,\theta)=\frac{1}{\lambda}\frac{\partial\mathfrak{J}_{i,\rho}}{\partial\rho}+\frac{2}{(1+\lambda\rho)}\mathfrak{J}_{i,\rho}+\frac{1}{(1+\lambda\rho)}\left(\frac{\partial}{\partial\theta}+\cot\theta\right)\mathfrak{J}_{i,\theta}, \tag{B 14}$$

from which performing an expansion in λ and equating terms order by order gives the following equations at order,

$$\lambda^{-2}:\quad \frac{\partial\mathfrak{J}^{(-1)}_{i,\rho}}{\partial\rho}=0,\quad\Rightarrow\quad \mathfrak{J}^{(-1)}_{i,\rho}(\rho,\theta)=\mathfrak{h}_i(\theta), \tag{B 15}$$

$$\lambda^{-1}:\quad \frac{\partial\mathfrak{J}^{(0)}_{i,\rho}}{\partial\rho}+2\mathfrak{J}^{(-1)}_{i,\rho}=0,\quad\Rightarrow\quad \mathfrak{J}^{(0)}_{i,\rho}(\rho,\theta)=g_i(\theta)+2\mathfrak{h}_i(\theta)\rho, \tag{B 16}$$

$$\lambda^{0}:\quad \frac{\partial\mathfrak{J}^{(1)}_{i,\rho}}{\partial\rho}+2\mathfrak{J}^{(0)}_{i,\rho}-2\rho\mathfrak{J}^{(-1)}_{i,\rho}+\left(\frac{\partial}{\partial\theta}+\cot\theta\right)\left(\mathfrak{J}^{(0)}_{i,\theta}-\rho\mathfrak{J}^{(-1)}_{i,\rho}\right)=0, \tag{B 17}$$

where $\mathfrak{h}_i(\theta)$, $g_i(\theta)$ are arbitrary functions of θ. Matching the currents in the inner and outer regions,

$$\mathfrak{h}_i(\theta)=\lim_{\lambda\to0,\rho\to\infty}\mathfrak{J}^{(-1)}_{i,\rho}(\rho,\theta)=\lim_{r\to1,\lambda\to0}\hat{\boldsymbol{n}}\cdot\boldsymbol{J}^{(-1)}_i(r,\theta)=0, \tag{B 18}$$

which implies $\mathfrak{h}_i(\theta)=0$ for all the species. Furthermore, the matching at the next order gives

$$g_i(\theta)=\mathfrak{J}^{(0)}_{i,\rho}(\rho=0,\theta)=\lim_{\lambda\to0,\rho\to\infty}\mathfrak{J}^{(0)}_{i,\rho}(\rho,\theta)=\lim_{r\to1,\lambda\to0}\hat{\boldsymbol{n}}\cdot\boldsymbol{J}^{(0)}_i(r,\theta), \tag{B 19}$$

providing the solution $g_i(\theta)=\mathcal{J}_i(\theta)K(\cos\theta)$; where $\mathcal{J}_i(\theta)$ are defined in appendix A and $K(\cos\theta)$ is defined in (2.10). Therefore, the outer flux boundary conditions at leading order are,

$$\hat{\boldsymbol{n}}\cdot\boldsymbol{J}_i(r=1,\theta)=g_i(\theta)=\begin{cases}\mathcal{J}_h(\theta)K(\cos\theta); & i=h,\ \text{(protons)},\\ 0; & i\in\{oh,\ s\pm\}.\end{cases} \tag{B 20}$$

In the following we drop the $^{(0)}$ subscript for the outer fluxes as we are interested only in the leading-order contributions (i.e. we have set $\boldsymbol{J}^{(n)}_i=0$ for $n\geqslant1$).

Next, we obtain the concentration profiles by first matching the inner fields with the $O(1)$ outer fields $C_i(r,\theta)$, $\Phi(r,\theta)$;

$$\lim_{\lambda\to0;\rho\to\infty}\{\mathcal{C}^{(0)}_i,\varphi^{(0)}\}(\rho,\theta)=\lim_{r\to1;\lambda\to0}\{C^{(0)}_i,\Phi^{(0)}\}(r,\theta)=\{C_i,\Phi\}(1,\theta). \tag{B 21}$$

Integrating (B 11) and using equations (B 15), (B 18) and (B 21), we obtain the leading-order concentration profile

$$1+\mathcal{C}_i^{(0)}(\rho,\theta)=(1+C_i(1,\theta))\,\mathrm{e}^{-(\varphi^{(0)}(\rho,\theta)-\Phi(1,\theta))}. \tag{B 22}$$

This method can be iterated to obtain the higher-order concentration fields such as $\mathcal{C}^{(1)}(\rho,\theta)$ from (B 17) above.

B.2. *Electric field*

Writing out Poisson's equation, in spherical polar coordinates,

$$-\lambda^2\left(\frac{1}{r^2}\frac{\partial}{\partial r}r^2\frac{\partial}{\partial r}+\frac{1}{r^2\sin\theta}\frac{\partial}{\partial\theta}\sin\theta\frac{\partial}{\partial\theta}\right)\Phi(r,\theta)=\sum_{i\in\{h,oh,s\pm\}}\mathcal{Z}_iC_i, \tag{B 23}$$

which at the leading order in the inner expansion reduces to

$$-\frac{\partial^2\varphi^{(0)}}{\partial\rho^2}=\sum_i\mathcal{Z}_i\mathcal{C}_i^{(0)}. \tag{B 24}$$

Substituting the concentration profiles from (B 22) into to the foregoing (B 24), we have

$$-\frac{\partial^2\varphi^{(0)}}{\partial\rho^2}=\sum_{i\in\{h,oh,s\pm\}}\mathcal{Z}_i(1+C_i(1,\theta))\mathrm{e}^{-z_i(\varphi^{(0)}(\rho,\theta)-\Phi(1,\theta))}. \tag{B 25}$$

In addition, applying electroneutrality in the outer region (see (3.19) in the main text) at leading order,

$$\sum_{i\in\{h,oh,s\pm\}}\mathcal{Z}_iC_i=0, \tag{B 26}$$

leads to the simpler expression

$$\frac{\partial^2\varphi^{(0)}}{\partial\rho^2}=C_s^*(\theta)\sinh\left(\varphi^{(0)}(\rho,\theta)-\Phi(1,\theta)\right), \tag{B 27}$$

where we have defined

$$C_s^*(\theta)=2\sum_{i\in\{h,s+\}}\mathcal{Z}_i\left(1+C_i(1,\theta)\right). \tag{B 28}$$

Introducing a convenient factor

$$2\frac{\partial\varphi^{(0)}}{\partial\rho}\frac{\partial^2\varphi^{(0)}}{\partial\rho^2}=2C_s^*\frac{\partial\varphi^{(0)}}{\partial\rho}\sinh\left(\varphi^{(0)}(\rho,\theta)-\Phi(1,\theta)\right) \tag{B 29}$$

and integrating once gives

$$\left(\frac{\partial\varphi^{(0)}}{\partial\rho}\right)^2=2C_s^*\left[\cosh\left(\varphi^{(0)}(\rho,\theta)-\Phi(1,\theta)\right)-1\right], \tag{B 30}$$

where the matching condition $\partial_\rho \varphi^{(0)}(\rho \to \infty, \theta) = 0$ (since the outer electric field expansion begins at $O(1)$) was applied. Thus, we obtain the electric field in the Debye layer using the identity $(2\sinh^2(x/2) = \cosh(x) - 1)$,

$$-\frac{\partial \varphi^{(0)}}{\partial \rho} = 2\sqrt{C_s^*}\sinh\left(\frac{\varphi^{(0)}(\rho,\theta) - \Phi(1,\theta)}{2}\right). \tag{B 31}$$

Integrating once again, we obtain

$$\frac{1}{2}\ln\left[\frac{\cosh\left(\left[\varphi^{(0)}(\rho',\theta) - \Phi(1,\theta)\right]/2\right) - 1}{\cosh\left(\left[\varphi^{(0)}(\rho',\theta) - \Phi(1,\theta)\right]/2\right) + 1}\right]_{\rho'=0}^{\rho'=\rho} = -\sqrt{C_s^*}\rho. \tag{B 32}$$

Now, using the hyperbolic identities $2\begin{Bmatrix}\sinh\\ \cosh\end{Bmatrix}^2(x/2) = \cosh(x) \mp 1$, we obtain (Anderson 1989; Yariv 2011)

$$\tanh\left(\frac{\varphi^{(0)}(\rho,\theta) - \Phi(1,\theta)}{4}\right) = \tanh\left(\frac{\zeta(\theta)}{4}\right)e^{-\sqrt{C_s^*}\rho}, \tag{B 33}$$

where $\zeta(\theta) = \varphi_s - \Phi(1,\theta)$.

B.3. *Momentum conservation*

Writing the Stokes equations in spherical polar coordinates,

$$(\nabla\cdot\boldsymbol{\Pi})\cdot\hat{\boldsymbol{e}}_r = \nabla^2 v_r - \frac{2v_r}{r^2} - \frac{2}{r^2\sin\theta}\frac{\partial}{\partial\theta}(\sin\theta\, v_\theta) - \frac{\partial p}{\partial r} + \frac{\partial\Phi}{\partial r}\nabla^2\Phi = 0, \tag{B 34}$$

$$(\nabla\cdot\boldsymbol{\Pi})\cdot\hat{\boldsymbol{e}}_\theta = \nabla^2 v_\theta - \frac{v_\theta}{r^2\sin^2\theta} + \frac{2}{r^2}\frac{\partial v_r}{\partial\theta} - \frac{1}{r}\frac{\partial p}{\partial\theta} + \frac{1}{r}\frac{\partial\Phi}{\partial\theta}\nabla^2\Phi = 0, \tag{B 35}$$

$$\nabla\cdot\boldsymbol{v} = \frac{\partial v_r}{\partial r} + \frac{2v_r}{r} + \frac{1}{r\sin\theta}\frac{\partial}{\partial\theta}(\sin\theta\, v_\theta) = 0. \tag{B 36}$$

To the leading order in the inner expansion (see (B 2)–(B 4)), the static pressure balances the electrostatic stresses normal to the surface (Anderson 1989; Yariv 2011)

$$\hat{\boldsymbol{e}}_\rho : \lambda^{-3}\left(-\frac{\partial\mathcal{P}^{(-2)}}{\partial\rho} - \sum_i \mathcal{Z}_i\mathcal{C}_i^{(0)}\frac{\partial\varphi^{(0)}}{\partial\rho}\right) + \lambda^{-2}\frac{\partial^2\mathcal{V}_\rho^{(0)}}{\partial\rho^2} + O\left(\lambda^{-1}\right) = 0. \tag{B 37}$$

Note that the expansion for the pressure field begins at $\mathcal{P}^{(-2)}$ to balance $O(\lambda^{-2})$ radial electric stresses that cannot be accounted by the viscous stresses (Anderson 1989; Yariv 2011). The viscous stresses balances the static pressure gradient and tangential electric stresses along the surface

$$\hat{\boldsymbol{e}}_\theta : \lambda^{-2}\left(\frac{\partial^2\mathcal{V}_\theta^{(0)}}{\partial\rho^2} - \frac{\partial\mathcal{P}^{(-2)}}{\partial\theta} - \sum_i \mathcal{Z}_i\mathcal{C}_i^{(0)}\frac{\partial\varphi^{(0)}}{\partial\theta}\right) + O\left(\lambda^{-1}\right) = 0, \tag{B 38}$$

with the leading-order incompressibility constraint

$$\lambda^{-1}\frac{\partial\mathcal{V}_\rho^{(0)}}{\partial\rho} + O(1) = 0. \tag{B 39}$$

Therefore, to leading $O(\lambda^{-3})$ in (B 37), the static pressure balances the radial electrostatic stress

$$-\frac{\partial \mathcal{P}^{(-2)}}{\partial \rho}-\sum_i \mathcal{Z}_i \mathcal{C}_i^{(0)} \frac{\partial \varphi^{(0)}}{\partial \rho}=0, \tag{B 40}$$

which gives the static pressure field

$$\mathcal{P}^{(-2)}(\rho,\theta)=2C_s^*(\theta)\sinh^2\left(\frac{\varphi^{(0)}(\rho,\theta)-\Phi(1,\theta)}{2}\right), \tag{B 41}$$

where matching with the outer solution implies $\mathcal{P}^{(-2)}(\infty,\theta)=0$ (since the outer field p expansion begins at $O(1)$). The next-order $O(\lambda^{-2})$ in (B 37), momentum balance is

$$\frac{\partial^2 \mathcal{V}_\rho^{(0)}}{\partial \rho^2}=0, \tag{B 42}$$

where the continuity equation (B 39), $\partial_\rho \mathcal{V}_\rho^{(0)}=0$ (i.e. $\mathcal{V}_\rho^{(0)}$ is ρ independent), implies

$$\mathcal{V}_\rho^{(0)}(\rho,\theta)=\boldsymbol{U}^e\cdot\hat{\boldsymbol{e}}_\rho. \tag{B 43}$$

At $O(\lambda^{-2})$ in (B 38), viscous stresses balance the tangential pressure gradient $\partial_\theta \mathcal{P}^{(-2)}$ and the tangential electrical stress;

$$\frac{\partial^2 \mathcal{V}_\theta^{(0)}}{\partial \rho^2}-\frac{\partial \mathcal{P}^{(-2)}}{\partial \theta}-\sum_i \mathcal{Z}_i \mathcal{C}_i^{(0)} \frac{\partial \varphi^{(0)}}{\partial \theta}=0. \tag{B 44}$$

Using (B 41) and (B 27), we obtain

$$\begin{aligned}\frac{\partial^2 \mathcal{V}_\theta^{(0)}}{\partial \rho^2} &= 2\sinh^2(2\varphi)\frac{\partial C_s^*}{\partial \theta}-2C_s^*\sinh(2\varphi)\cosh(2\varphi)\\ &= \frac{2\tanh(2\varphi)}{1-\tanh^2(2\varphi)}\left[\tanh(2\varphi)\frac{\partial C_s^*}{\partial \theta}+C_s^*\frac{\partial \Phi}{\partial \theta}\right],\end{aligned} \tag{B 45}$$

where $4\varphi(\rho,\theta)=\varphi^{(0)}(\rho,\theta)-\Phi(1,\theta)$. Using the identity $\tanh(2x)=2\tanh(x)/(1+\tanh^2(x))$,

$$\frac{\partial^2 \mathcal{V}_\theta^{(0)}}{\partial \rho^2}=2\left[\frac{4\tanh^2(\varphi)\frac{\partial C_s^*}{\partial \theta}}{(1+\tanh(\varphi))^2(1-\tanh(\varphi))^2}-\frac{2\tanh(\varphi)C_s^*\frac{\partial \Phi}{\partial \theta}}{(1+\tanh(\varphi))^2(1-\tanh(\varphi))^2}\right]. \tag{B 46}$$

It is helpful to write the coefficients of the right-hand side first and second terms as

$$\begin{aligned}\frac{4\tanh^2(\varphi)}{(1+\tanh(\varphi))^2(1-\tanh(\varphi))^2} &= \frac{-1}{(1+\tanh(\varphi))}+\frac{1}{(1+\tanh(\varphi))^2}\\ &\quad+\frac{-1}{(1-\tanh(\varphi))}+\frac{1}{(1-\tanh(\varphi))^2},\end{aligned} \tag{B 47}$$

$$\frac{2\tanh(\varphi)}{(1+\tanh(\varphi))^2(1-\tanh(\varphi))^2} = \frac{1}{(1+\tanh(\varphi))} + \frac{-1}{(1+\tanh(\varphi))^2} + \frac{-1}{(1-\tanh(\varphi))} + \frac{1}{(1-\tanh(\varphi))^2}. \tag{B 48}$$

Using (B 33) and integrating once, we obtain

$$\frac{\partial \mathcal{V}_\theta^{(0)}}{\partial \rho} = \frac{2}{\sqrt{C_s^*}}\left[\frac{2Q^2}{\left(Q^2 - e^{2\sqrt{C_s^*}\rho}\right)}\frac{\partial \mathcal{C}^*}{\partial \theta} - \frac{2Qe^{\sqrt{C_s^*}\rho}}{\left(Q^2 - e^{2\sqrt{C_s^*}\rho}\right)}C_s^*\frac{\partial \Phi}{\partial \theta}\right], \tag{B 49}$$

where $Q = \tanh(\zeta(\theta)/4)$ and such that matching with the outer solution imposes $\partial_\rho \mathcal{V}_\theta^{(0)}(\infty, \theta) = 0$. In obtaining the above expression, we have used the following integral identities

$$\int \frac{\mathrm{d}\rho'}{1 + Qe^{-\sqrt{C_s^*}\rho'}} = \frac{1}{\sqrt{C_s^*}}\ln\left(Q + e^{\sqrt{C_s^*}\rho}\right) + \text{const.}, \tag{B 50}$$

$$\int \frac{\mathrm{d}\rho'}{\left(1 + Qe^{-\sqrt{C_s^*}\rho'}\right)^2} = \frac{1}{\sqrt{C_s^*}}\frac{Q}{\left(Q + e^{\sqrt{C_s^*}}\right)} + \frac{1}{\sqrt{C_s^*}}\ln\left(Q + e^{\sqrt{C_s^*}\rho}\right) + \text{const.}, \tag{B 51}$$

$$\int \frac{\mathrm{d}\rho'}{1 - Qe^{-\sqrt{C_s^*}\rho'}} = \frac{1}{\sqrt{C_s^*}}\ln\left(e^{\sqrt{C_s^*}\rho} - Q\right) + \text{const.}, \tag{B 52}$$

$$\int \frac{\mathrm{d}\rho'}{\left(1 - Qe^{-\sqrt{C_s^*}\rho'}\right)^2} = -\frac{1}{\sqrt{C_s^*}}\frac{Q}{\left(Q + e^{\sqrt{C_s^*}}\right)} + \frac{1}{\sqrt{C_s^*}}\ln\left(e^{\sqrt{C_s^*}\rho} - Q\right) + \text{const.} \tag{B 53}$$

Finally, integrating again,

$$\mathcal{V}_\theta^{(0)}(\rho, \theta) = \mathcal{V}_\theta^{(0)}(0, \theta) + \frac{2}{C_s^*}\frac{\partial C_s^*}{\partial \theta}\ln\left(\frac{1 - Q^2e^{-2\rho\sqrt{C_s^*}}}{1 - Q^2}\right) - 4\frac{\partial \Phi}{\partial \theta}\left(\tanh^{-1}\left(Qe^{-\sqrt{C_s^*}\rho}\right) - \tanh^{-1}(Q)\right). \tag{B 54}$$

Therefore, in the thin-layer limit $\lambda \to 0$ and $\rho \to \infty$,

$$\lim_{\lambda\to 0;\rho\to\infty} \mathcal{V}_\theta^{(0)}(\rho, \theta) = \mathcal{V}_\theta^{(0)}(0, \theta) + \zeta(\theta)\frac{\partial \Phi}{\partial \theta} - \frac{2}{C_s^*}\frac{\partial C_s^*}{\partial \theta}\ln\left(1 - \tanh^2\left(\frac{\zeta(\theta)}{4}\right)\right). \tag{B 55}$$

Finally, matching with the leading-order outer flow field

$$\lim_{\lambda\to 0;\rho\to\infty} \mathcal{V}_\theta^{(0)}(\rho, \theta) = \lim_{r\to 1,\lambda\to 0} \boldsymbol{v}^{(0)}(r, \theta) = \boldsymbol{v}(1, \theta), \tag{B 56}$$

we obtain the slip velocity boundary condition for the outer flow (Anderson *et al.* 1982; Yariv 2011)

$$\boldsymbol{v}(1, \theta) = \boldsymbol{U}^e + \left[\zeta(\theta)\frac{\partial \Phi}{\partial \theta} + 4\frac{\partial \ln C_s^*}{\partial \theta}\ln\cosh\left(\frac{\zeta(\theta)}{4}\right)\right]\hat{\boldsymbol{e}}_\theta. \tag{B 57}$$

REFERENCES

ANDERSON, J. L. 1989 Colloidal transport by interfacial forces. *Annu. Rev. Fluid Mech.* **21**, 61–99.

ANDERSON, J. L., LOWELL, M. E. & PRIEVE, D. C. 1982 Motion of a particle generated by chemical gradients part 1. Non-electrolytes. *J. Fluid Mech.* **117**, 107–121.

BALASUBRAMANIAN, S., KAGAN, D., MANESH, K. M., CALVO-MARZAL, P., FLECHSIG, G. U. & WANG, J. 2009 Thermal modulation of nanomotor movement. *Small* **5**, 1569–1574.

BRADY, J. F. 2011 Particle motion driven by solute gradients with application to autonomous motion: continuum and colloidal perspectives. *J. Fluid Mech.* **667**, 216–259.

BRICARD, A., CAUSSIN, J.-B., DESREUMAUX, N., DAUCHOT, O. & BARTOLO, D. 2013 Emergence of macroscopic directed motion in populations of motile colloids. *Nature* **503** (7474), 95–98.

BROWN, A. & POON, W. 2014 Ionic effects in self-propelled Pt-coated Janus swimmers. *Soft Matt.* **10** (22), 4016–4027.

CHANDRASEKHAR, S. 1943 Stochastic problems in physics and astronomy. *Rev. Mod. Phys.* **15**, 1–89.

DAS, S., GARG, A., CAMPBELL, A. I., HOWSE, J. R., SEN, A., VELEGOL, D., GOLESTANIAN, R. & EBBENS, S. J. 2015 Boundaries can steer active Janus spheres. *Nat. Commun.* **6**, 8999.

DHAR, P., FISCHER, TH. M., WANG, Y., MALLOUK, T. E., PAXTON, W. F. & SEN, A. 2006 Autonomously moving nanorods at a viscous interface. *Nano Lett.* **6** (1), 66–72.

EBBENS, S., GREGORY, D. A., DUNDERDALE, G., HOWSE, J. R., IBRAHIM, Y., LIVERPOOL, T. B. & GOLESTANIAN, R. 2014 Electrokinetic effects in catalytic Pt-insulator Janus swimmers. *Europhys. Lett.* **106**, 58003.

EBBENS, S., TU, M.-H., HOWSE, J. R. & GOLESTANIAN, R. 2012 Size dependence of the propulsion velocity for catalytic Janus-sphere swimmers. *Phys. Rev.* E **85** (2), 020401.

FARNIYA, A. A., ESPLANDIU, M. J., REGUERA, D. & BACHTOLD, A. 2013 Imaging the proton concentration and mapping the spatial distribution of the electric field of catalytic micropumps. *Phys. Rev. Lett.* **111** (October), 1–5.

GIBBS, J. G. & ZHAO, Y. P. 2009 Autonomously motile catalytic nanomotors by bubble propulsion. *Appl. Phys. Lett.* **94** (16), 163104(3).

GOLESTANIAN, R., LIVERPOOL, T. & AJDARI, A. 2005 Propulsion of a molecular machine by asymmetric distribution of reaction products. *Phys. Rev. Lett.* **94** (22), 1–4.

GOLESTANIAN, R., LIVERPOOL, T. B. & AJDARI, A. 2007 Designing phoretic micro- and nano-swimmers. *New J. Phys.* **9** (5), 126–126.

HALL, S., KHUDAISH, E. A. & HART, A. L. 1998 Electrochemical oxidation of hydrogen peroxide at platinum electrodes. Part II: effect of potential. *Electrochim. Acta* **43** (14–15), 2015–2024.

HALL, S. B., KHUDAISH, E. A. & HART, A. L. 1999*a* Electrochemical oxidation of hydrogen peroxide at platinum electrodes. Part III: effect of temperature. *Electrochim. Acta* **44** (14), 2455–2462.

HALL, S. B., KHUDAISH, E. A. & HART, A. L. 1999*b* Electrochemical oxidation of hydrogen peroxide at platinum electrodes. Part IV: phosphate buffer dependence. *Electrochim. Acta* **44** (25), 4573–4582.

HALL, S. B., KHUDAISH, E. A. & HART, A. L. 2000 Electrochemical oxidation of hydrogen peroxide at platinum electrodes. Part V: inhibition by chloride. *Electrochim. Acta* **45**, 3573–3579.

HOWSE, J., JONES, R., RYAN, A., GOUGH, T., VAFABAKHSH, R. & GOLESTANIAN, R. 2007 Self-motile colloidal particles: from directed propulsion to random walk. *Phys. Rev. Lett.* **99** (4), 048102.

JACKSON, J. D. 1975 *Classical Electrodynamics*. Wiley.

KAGAN, D., CALVO-MARZAL, P., BALASUBRAMANIAN, S., SATTAYASAMITSATHIT, S., MANESH, K. M., FLECHSIG, G.-U. & WANG, J. 2009 Chemical sensing based on catalytic nanomotors: motion-based detection of trace silver. *J. Am. Chem. Soc.* **131** (34), 12082.

KAPRAL, R. 2013 Perspective: nanomotors without moving parts that propel themselves in solution. *J. Chem. Phys.* **138** (2), 020901.

KATSOUNAROS, I., SCHNEIDER, W. B., MEIER, J. C., BENEDIKT, U., BIEDERMANN, P. U., AUER, A. A. & MAYRHOFER, K. J. J. 2012 Hydrogen peroxide electrochemistry on platinum:

towards understanding the oxygen reduction reaction mechanism. *Phys. Chem. Chem. Phys.* **14**, 73847391.

KLINE, T. R., PAXTON, W. F., MALLOUK, T. E. & SEN, A. 2005*a* Catalytic nanomotors: remote-controlled autonomous movement of striped metallic nanorods. *Angew. Chem. Intl Ed. Engl.* **44** (5), 744–746.

KLINE, T. R., PAXTON, W. F., WANG, Y., VELEGOL, D., MALLOUK, T. E. & SEN, A. 2005*b* Catalytic micropumps: microscopic convective fluid flow and pattern formation. *J. Am. Chem. Soc.* **127** (49), 17150-1.

KÜMMEL, F., TEN HAGEN, B., WITTKOWSKI, R., BUTTINONI, I., EICHHORN, R., VOLPE, G., LÖWEN, H. & BECHINGER, C. 2013 Circular motion of asymmetric self-propelling particles. *Phys. Rev. Lett.* **110** (19), 198302.

LAMB, H. 1932 *Hydrodynamics*, 6th edn. Cambridge University Press.

LIU, Y., WU, H., LI, M., YIN, J.-J. & NIE, Z. 2014 pH dependent catalytic activities of platinum nanoparticles with respect to the decomposition of hydrogen peroxide and scavenging of superoxide and singlet oxygen. *Nanoscale* **6** (20), 11904–11910.

MARCHETTI, M. C., JOANNY, J. F., RAMASWAMY, S., LIVERPOOL, T. B., PROST, J., RAO, M. & SIMHA, R. A. 2013 Hydrodynamics of soft active matter. *Rev. Mod. Phys.* **85** (3), 1143–1189.

MCKEE, D. W. 1969 Catalytic decomposition of hydrogen peroxide by metals and alloys of the platinum group. *J. Catalysis* **14** (4), 355–364.

MICHELIN, S. & LAUGA, E. 2014 Phoretic self-propulsion at finite Péclet numbers. *J. Fluid Mech.* **747**, 572–604.

MORAN, J. L. & POSNER, J. D. 2011 Electrokinetic locomotion due to reaction-induced charge auto-electrophoresis. *J. Fluid Mech.* **680**, 31–66.

PAGONABARRAGA, I., ROTENBERG, B. & FRENKEL, D. 2010 Recent advances in the modelling and simulation of electrokinetic effects: bridging the gap between atomistic and macroscopic descriptions. *Phys. Chem. Chem. Phys.* **12** (33), 9566–9580.

PALACCI, J., SACANNA, S., STEINBERG, A. P., PINE, D. J & CHAIKIN, P. M. 2013 Living crystals of light-activated colloidal surfers. *Science* **339** (6122), 936–940.

PATRA, D., SENGUPTA, S., DUAN, W., ZHANG, H., PAVLICK, R. & SEN, A. 2013 Intelligent, self-powered, drug delivery systems. *Nanoscale* **5** (4), 1273–1283.

PAXTON, W. F., SEN, A. & MALLOUK, T. E. 2005 Motility of catalytic nanoparticles through self-generated forces. *Chemistry* **11** (22), 6462–6470.

POPESCU, M. N., DIETRICH, S. & OSHANIN, G. 2009 Confinement effects on diffusiophoretic self-propellers. *J. Chem. Phys.* **130** (19), 194702.

PRIEVE, D. C., ANDERSON, J. L., EBEL, J. E. & LOWELL, M. E. 1984 Motion of a particle generated by chemical gradients part 2. Electrolytes. *J. Fluid Mech.* **148**, 247–269.

PROBSTEIN, R. 2003 *Physicochemical Hydrodynamics*, 2nd edn. Wiley.

RÜCKNER, G. & KAPRAL, R. 2007 Chemically powered nanodimers. *Phys. Rev. Lett.* **98** (15), 150603.

RUSSEL, W. B., SAVILLE, D. A. & SCHOWALTER, W. R. 1992 *Colloidal Dispersions*, 2nd edn. Cambridge University Press.

SABASS, B. & SEIFERT, U. 2010 Efficiency of surface-driven motion: nanoswimmers beat microswimmers. *Phys. Rev. Lett.* **105** (November), 1–4.

SABASS, B. & SEIFERT, U. 2012 Nonlinear, electrocatalytic swimming in the presence of salt. *J. Chem. Phys.* **136** (21), 214507.

SHARIFI-MOOD, N., KOPLIK, J. & MALDARELLI, C. 2013 Diffusiophoretic self-propulsion of colloids driven by a surface reaction: the sub-micron particle regime for exponential and van der Waals interactions. *Phys. Fluids* **25** (1), 012001.

THEURKAUFF, I., COTTIN-BIZONNE, C., PALACCI, J., YBERT, C. & BOCQUET, L. 2012 Dynamic clustering in active colloidal suspensions with chemical signaling. *Phys. Rev. Lett.* **108** (26), 268303.

VALADARES, L. F., TAO, Y. G., ZACHARIA, N. S., KITAEV, V., GALEMBECK, F., KAPRAL, R. & OZIN, G. A. 2010 Catalytic nanomotors: self-propelled sphere dimers. *Small* **6** (4), 565–572.

VOLPE, G., BUTTINONI, I., VOGT, D., KÜMMERER, H.-J. & BECHINGER, C. 2011 Microswimmers in patterned environments. *Soft Matt.* **7** (19), 8810.

WANG, Y., HERNANDEZ, R. M., BARTLETT, D. J., BINGHAM, J. M., KLINE, T. R., SEN, A. & MALLOUK, T. E. 2006 Bipolar electrochemical mechanism for the propulsion of catalytic nanomotors in hydrogen peroxide solutions. *Langmuir* **22** (25), 10451–10456.

YARIV, E. 2011 Electrokinetic self-propulsion by inhomogeneous surface kinetics. *Proc. R. Soc. Lond.* A **467** (2130), 1645–1664.

ZHAO, G., SANCHEZ, S., SCHMIDT, O. G. & PUMERA, M. 2013 Poisoning of bubble propelled catalytic micromotors: the chemical environment matters. *Nanoscale* **5** (7), 2909–2914.